Interaction Notes

Note 327

STICK-MODEL CHARACTERIZATION OF THE TOTAL AXIAL
CURRENT AND LINEAR CHARGE DENSITY ON THE SURFACE OF
AN AIRCRAFT SUBJECTED TO AN EMP: FREQUENCY-DOMAIN
EXTERNAL-INTERACTION CURRENT AND CHARGE TRANSFER FUNCTIONS

September 13, 1977

G. Bedrosian

DIKEWOOD INDUSTRIES, INC.
Albuquerque, New Mexico

Abstract

The six-length stick model of the aircraft is used to find the frequency-
domain external-interaction current and charge transfer functions of the sur-
face of an aircraft. The resulting functions are plotted for three particular
aircraft: the B-1, the E-4, and the EC-135.

$AFWL-TR-77-175$

Distribution limited to U.S.
Government Agencies

Interaction Notes

Note 327

STICK-MODEL CHARACTERIZATION OF THE TOTAL AXIAL
CURRENT AND LINEAR CHARGE DENSITY ON THE SURFACE OF
AN AIRCRAFT SUBJECTED TO AN EMP: FREQUENCY-DOMAIN
EXTERNAL-INTERACTION CURRENT AND CHARGE TRANSFER FUNCTIONS

September 13, 1977

G. Bedrosian

DIKEWOOD INDUSTRIES, INC.
Albuquerque, New Mexico

Abstract

     The six-length stick model of the aircraft is used to find the frequency-
domain external-interaction current and charge transfer functions of the sur-
face of an aircraft. The resulting functions are plotted for three particular
aircraft: the B-1, the E-4, and the EC-135.

SECTION I

INTRODUCTION

Reference 1 presents a general scheme whereby the total axial current on the surface of an aircraft can be estimated using a "six-length stick model," where the six lengths are the forward fuselage (ℓ_1), the port and starboard wings (ℓ_2), the aft fuselage (ℓ_3), the bottom section of the vertical stabilizer (ℓ_4), the port and starboard horizontal stabilizers (ℓ_5), and the top section of the vertical stabilizer (ℓ_6) (see figure 1). In that report, a linear system of equations was developed from junction and end conditions on the sticks (see table 1). The zeros of the determinant of this system of equations give the real parts of the aircraft natural frequencies. The corresponding imaginary (damping) parts of the aircraft natural frequencies can be readily calculated using the methods presented in reference 1.

This report will continue the method of reference 1 by solving the linear system of equations with an impulse incident field. The resulting external-interaction current and charge transfer functions are then expanded in Mittag-Leffler series and the poles are shifted into the upper half ω-plane according to the previously calculated imaginary parts of the aircraft natural frequencies. In this way, the resonances in the aircraft induced currents and charges are given their proper damping.

It should be emphasized that the external-interaction transfer functions can be multiplied by a particular frequency-domain excitation function in case the particular frequency-domain response is needed. For instance, if the impulse response is $I_\delta(\omega)$ and the time-domain excitation is

$$E(t) = E_o e^{-t/t_f} U(t)$$

then the particular frequency-domain response is

$$I(\omega) = \frac{E_o t_f}{1 + j\omega t_f} I_\delta(\omega)$$

2

It should also be remarked that the functions to be calculated are the total axial current and total linear charge density. The distribution of the total current (charge) as a function of position on the circumference of each section is a separate problem. A very simplistic solution, valid in the low-frequency limit and away from junctions, is presented as an example of how to combine the local circumferential distribution with the global total current to obtain the current density at each point on the aircraft surface.

Numerical results are obtained for three aircraft: the B-1, the E-4, and the EC-135. The total current and charge are plotted versus frequency for several points of interest on the three aircraft for topside incidence of the external EMP. A preliminary comparison is made with data calculated using another technique, and the agreement is in general quite reasonable. The FORTRAN computer code used to generate the numerical results is presented in appendix B.

Many schemes have been previously formulated to obtain numerical results for the frequency-domain charge and current transfer functions on the surface of an aircraft [refs. 5 and 6]. While the numerical efficiency of this particular method (both in computer memory requirement and computational speed) would perhaps be justification enough for its addition to the growing number of computer programs which approximate the current and charge on aircraft surfaces, the true value of the stick-model transfer functions is that they are available in simple analytical form, which greatly simplifies the tasks of Fourier inversion into the time domain and synthesis of equivalent networks. These tasks should be the subject of future research.

SECTION II
UNDAMPED SOLUTION

As presented in reference 1, the current on each of the six sections of the stick model of the aircraft (see figure 1) can be written

$$I_1 = I_{ind}(k,x,\theta) + S_1 \sin[k(x-\ell_1-\ell_3)] - I_{ind}(k, \ell_1+\ell_3, \theta)\cos[k(x-\ell_1-\ell_3)]$$

$$I_2 = S_2 \sin[k(y-\ell_2)] \qquad (y > 0)$$

$$I_3 = I_{ind}(k,x,\theta) + S_3 \sin[k(x-\ell_3)] + C_3 \cos[k(x-\ell_3)]$$

$$I_4 = - I_{ind}(k,z, \pi/2 - \theta) + S_4 \sin[k(z-\ell_4)] + C_4 \cos[k(z-\ell_4)] \qquad (1)$$

$$I_5 = S_5 \sin[k(y-\ell_5)] \qquad (y > 0)$$

$$I_6 = - I_{ind}(k,z, \pi/2 - \theta) + S_6 \sin[k(z-\ell_4-\ell_6)]$$

$$+ I_{ind}(k, \ell_4+\ell_6, \pi/2 - \theta)\cos[k(z-\ell_4-\ell_6)]$$

where

$$I_{ind}(k,\xi,\phi) \equiv \frac{4\pi j E_o}{k Z_o \Omega \sin \phi} e^{jk \xi \cos \phi}$$

valid to first order in Ω^{-1}, where Ω is the overall stick-model parameter of the aircraft [ref. 1,2], k is the wave number, Z_o is the impedance of free space, θ is the angle of incidence, (x,y,z) is the position on the aircraft, and E_o is the strength of the impulse incident electric field.

The requirement that the current vanish at the free ends of the sticks is satisfied by equations (1). It is also required that the current be conserved and the quasi-static potential be continuous at the junctions. These junction conditions lead to matrix equation (2) (see table 1).
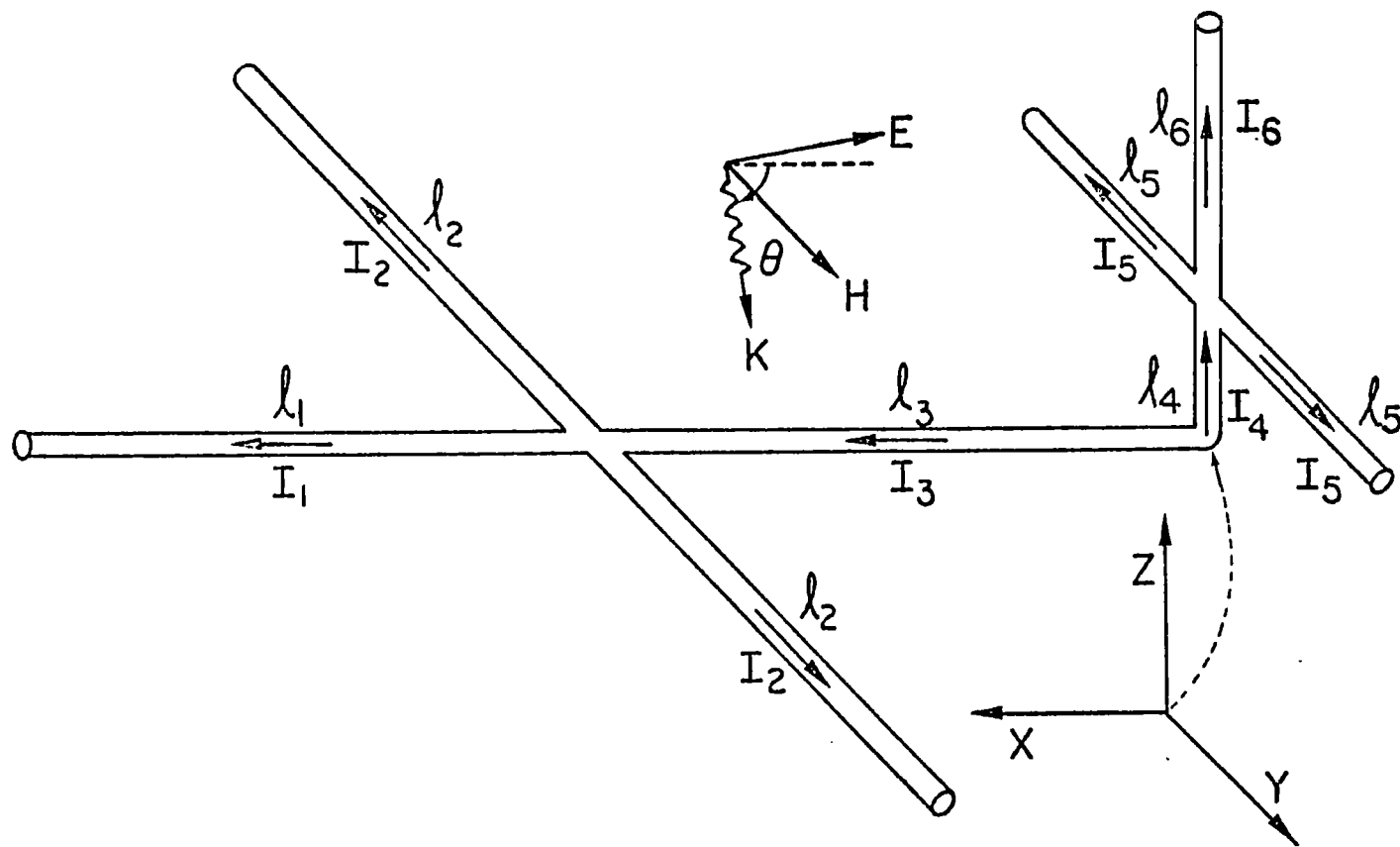
4

Figure 1. The six-length stick model.

Table 1.

MATRIX EQUATION (2)

$$\begin{bmatrix}
-\sin k\ell_1 & -2\sin k\ell_2 & 0 & -1 & 0 & 0 & 0 & 0 \\
\cos k\ell_1 & 0 & -1 & 0 & 0 & 0 & 0 & 0 \\
0 & \cos k\ell_2 & -1 & 0 & 0 & 0 & 0 & 0 \\
0 & 0 & -\sin k\ell_3 & \cos k\ell_3 & \cos k\ell_4 & -\sin k\ell_4 & 0 & 0 \\
0 & 0 & \cos k\ell_3 & \sin k\ell_3 & -\sin k\ell_4 & -\cos k\ell_4 & 0 & 0 \\
0 & 0 & 0 & 0 & 0 & -1 & \cos k\ell_5 & 0 \\
0 & 0 & 0 & 0 & 0 & -1 & 0 & \cos k\ell_6 \\
0 & 0 & 0 & 0 & -1 & 0 & -2\sin k\ell_5 & -\sin k\ell_6
\end{bmatrix}
\begin{bmatrix}
S_1 \\ S_2 \\ S_3 \\ C_3 \\ C_4 \\ S_4 \\ S_5 \\ S_6
\end{bmatrix}
= \frac{4\pi j E_o}{k\Omega Z_o}
\begin{bmatrix}
\cos k\ell_1 \csc\theta\, e^{jk(\ell_1+\ell_3)\cos\theta} \\
\sin k\ell_1 \csc\theta\, e^{jk(\ell_1+\ell_3)\cos\theta} \\
j\cot\theta\, e^{jk\ell_3\cos\theta} \\
\sec\theta - \csc\theta \\
-j(\tan\theta + \cot\theta) \\
-j\tan\theta\, e^{jk\ell_4\sin\theta} \\
-\sin k\ell_6 \sec\theta\, e^{jk(\ell_4+\ell_6)\sin\theta} \\
-\cos k\ell_6 \sec\theta\, e^{jk(\ell_4+\ell_6)\sin\theta}
\end{bmatrix}$$

It is evident from the symmetry of the physical situation as well as equations (1) that the solution of matrix equation (2) is unchanged under the transformation $n \to 7 - n$, $x \rightleftarrows z$, $\theta \to \pi/2 - \theta$, $E_o \to -E_o$. It is therefore sufficient to solve for I_1, I_2, and I_3; I_4, I_5, and I_6 can be found by symmetry.

After some lengthy arithmetic, one arrives at the following expressions for I_1, I_2, and I_3:

$$I_1 = \frac{4\pi j E_o}{k Z_o \Omega} \left\{ \frac{e^{jkx \cos \theta}}{\sin \theta} - \cos[k(x - \ell_1 - \ell_3)] F_1(k, \theta) \right.$$

$$\left. + \sin[k(x - \ell_1 - \ell_3)] \sum_{m=1}^{6} \psi_{1,m}(k) F_m(k, \theta) \right\}$$

$$I_2 = \frac{4\pi j E_o}{k Z_o \Omega} \left\{ \sin[k(y - \ell_2)] \sum_{m=1}^{6} \psi_{2,m}(k) F_m(k, \theta) \right\} \tag{3}$$

$$I_3 = \frac{4\pi j E_o}{k Z_o \Omega} \left\{ \frac{e^{jkx \cos \theta}}{\sin \theta} + \sin[k(x - \ell_3)] \sum_{m=1}^{6} \psi_{3,m}(k) F_m(k, \theta) \right.$$

$$\left. + \cos[k(x - \ell_3)] \sum_{m=1}^{6} \psi_{4,m}(k) F_m(k, \theta) \right\},$$

where

$$F_1 = \csc \theta \, e^{jk(\ell_1 + \ell_3) \cos \theta}$$

$$F_2 = 2j \cot \theta \, e^{jk\ell_3 \cos \theta}$$

$$F_3 = \sec \theta - \csc \theta$$

$$F_4 = -j(\tan \theta + \cot \theta)$$

7

$$F_5 = 2j \tan \theta \; e^{jk\ell_4 \sin \theta}$$

$$F_6 = \sec \theta \; e^{jk(\ell_4 + \ell_6) \sin \theta}$$

and $\psi_{r,m}$ are given in appendix A.

It would appear from equations (3) that the expressions for I_1, I_2, and I_3 become singular as $k \to 0$ and as $\theta \to n\pi/2$. However, this is not the case because of extensive cancellation as $k \to 0$ or as $\theta \to n\pi/2$. In fact, I is $O(k)$ as $k \to 0$, and I remains finite and continuous as $\theta \to n\pi/2$.

8

SECTION III
DAMPED SOLUTION

The ψ-functions of equations (3) have simple poles at the aircraft resonances, k_n. Each ψ-function consists of a numerator composed of cosine and sine functions and a common denominator, $D(k)$, which is

$$D(k) = \cos k\ell_1 \cos k\ell_2 \cos k(\ell_3+\ell_4)\cos k\ell_5 \cos k\ell_6$$

$$\times [\tan k\ell_1 + 2 \tan k\ell_2 + \tan k(\ell_3+\ell_4) + 2 \tan k\ell_5 + \tan k\ell_6$$

$$- (\tan k\ell_1 + 2 \tan k\ell_2)\tan k(\ell_3+\ell_4)(2 \tan k\ell_5 + \tan k\ell_6)] \ .$$

To introduce damping, one must expand $1/D(k)$ in a Mittag-Leffler series. However, care should be exercised to keep the first two terms of the Laurent expansion of $D(k)$ near $k = 0$ to insure proper low-frequency behavior:

$$1/[k\,D(k)] = Ak^{-2} + B + \ .\ .\ .$$

$$A = (\ell_1 + 2\ell_2 + \ell_3 + \ell_4 + 2\ell_5 + \ell_6)^{-1}$$

$$B = \frac{1}{2}[\ell_1^2 + \ell_2^2 + (\ell_3+\ell_4)^2 + \ell_5^2 + \ell_6^2]A$$

$$- \frac{1}{3}[\ell_1^3 + 2\ell_2^3 + (\ell_3+\ell_4)^3 + 2\ell_5^3 + \ell_6^3]A^2$$

$$+ (\ell_1 + 2\ell_2)(\ell_3+\ell_4)(2\ell_5 + \ell_6)A^2$$

The function, $1/[k\,D(k)] - Ak^{-2} - B$, is now conveniently Mittag-Leffler expanded [ref. 3] and the result is

$$\frac{1}{D(k)} = \frac{A}{k} + k\left\{B + \sum_{n=1}^{\infty} \frac{R_n}{k_n}\left[\left(\frac{1}{k-k_n} + \frac{1}{k_n}\right) - \left(\frac{1}{k+k_n} + \frac{1}{-k_n}\right)\right]\right\},$$

where k_n are the positive aircraft (real) resonances and

$$R_n = [\sec k_n \ell_1 \sec k_n \ell_2 \sec k_n(\ell_3+\ell_4)\sec k_n\ell_5 \sec k_n\ell_6] \div$$

$$[\ell_1 \sec^2 k_n\ell_1 + 2\ell_2\sec^2 k_n\ell_2 + (\ell_3+\ell_4)\sec^2 k_n(\ell_3+\ell_4) + 2\ell_5\sec^2 k_n\ell_5 + \ell_6\sec^2 k_n\ell_6$$

$$- (\ell_1\sec^2 k_n\ell_1 + 2\ell_2\sec^2 k_n\ell_2)\tan k_n(\ell_3+\ell_4)(2\tan k_n\ell_5 + \tan k_n\ell_6)$$

$$- (\tan k_n\ell_1 + 2\tan k_n\ell_2)(\ell_3+\ell_4)\sec^2 k_n(\ell_3+\ell_4)(2\tan k_n\ell_5 + \tan k_n\ell_6)$$

$$- (\tan k_n\ell_1 + 2\tan k_n\ell_2)\tan k_n(\ell_3+\ell_4)(2\ell_5\sec^2 k_n\ell_5 + \ell_6\sec^2 k_n\ell_6)] \ .$$

Damping is simply introduced by shifting the aircraft resonances into the upper-half k-plane by the respective damping factors; i.e., $\pm k_n \rightarrow \pm k_n + j\alpha_n$. The k_n's and α_n's are calculated using the methods of reference 1. The trigonometric expression for $1/D(k)$ should be replaced by

$$1/\hat{D}(k) = \frac{A}{k} + k\left\{B + \sum_{n=1}^{\infty} \frac{R_n}{k_n}\left[\left(\frac{1}{k-k_n-j\alpha_n} + \frac{1}{k_n+j\alpha_n}\right) - \left(\frac{1}{k+k_n-j\alpha_n} + \frac{1}{-k_n+j\alpha_n}\right)\right]\right\} \quad (4)$$

in each of the expressions for the ψ-functions (appendix A), giving the damped $\hat{\psi}$-functions.

One final step is necessary to preserve junction and end conditions. The leading terms in I_1 and I_3 in the undamped solution should be multiplied by unity, in the form $1 = D(k)/D(k)$. In the damped solution, this is transformed to $D(k)/\hat{D}(k)$. The damped expressions for I_1 , I_2 , and I_3 are finally

10

$$I_1 = \frac{4\pi jE_o}{kZ_o\Omega} \left\{ \left[\frac{e^{jkx\cos\theta}}{\sin\theta} - \cos[k(x-\ell_1-\ell_3)]F_1(k,\theta) \right] \frac{D(k)}{\hat{D}(k)} \right.$$

$$\left. + \sin[k(x-\ell_1-\ell_3)] \sum_{m=1}^{6} \hat{\psi}_{1,m}(k)F_m(k,\theta) \right\}$$

$$I_2 = \frac{4\pi jE_o}{kZ_o\Omega} \left\{ \sin[k(y-\ell_2)] \sum_{m=1}^{6} \hat{\psi}_{2,m}(k)F_m(k,\theta) \right\} \tag{5}$$

$$I_3 = \frac{4\pi jE_o}{kZ_o\Omega} \left\{ \frac{e^{jkx\cos\theta}}{\sin\theta} \frac{D(k)}{\hat{D}(k)} + \sin[k(x-\ell_3)] \sum_{m=1}^{6} \hat{\psi}_{3,m}(k)F_m(k,\theta) \right.$$

$$\left. + \cos[k(x-\ell_3)] \sum_{m=1}^{6} \hat{\psi}_{4,m}(k)F_m(k,\theta) \right\} .$$

This damping scheme provides for the correct behavior as $k \to 0$ and $\theta \to n\pi/2$, and for the satisfaction of junction and end conditions, regardless of the number of terms actually used in the approximation of $\hat{D}(k)$. This scheme also allows calculation of the strengths of the natural modes at the resonances. (Illustrations of the natural modes for the B-1, E-4, and EC-135 are available in reference 1.)

11

SECTION IV
LINEAR CHARGE DENSITY

The linear charge density and the total axial current are related by the continuity equation

$$\frac{\partial}{\partial \xi} I + \frac{\partial}{\partial t} \tau = 0$$

where ξ is the stick coordinate and τ is the linear charge density. Since the time-variation of τ is

$$\tau(t) = \tau(0)e^{j\omega t} = \tau(0)e^{jkct}$$

the linear charge density is given immediately from the axial current as

$$\tau = \frac{-1}{jkc} \frac{\partial I}{\partial \xi}$$

or

$$\tau_1 = \frac{-4\pi E_o}{kcZ_o\Omega} \left\{ \left[j \cot \theta \ e^{jkx \cos \theta} + \sin[k(x-\ell_1-\ell_3)]F_1(k,\theta) \right] \frac{D(k)}{\hat{D}(k)} \right.$$

$$\left. + \cos[k(x-\ell_1-\ell_3)] \sum_{m=1}^{6} \hat{\psi}_{1,m}(k)F_m(k,\theta) \right\} \tag{6}$$

$$\tau_2 = \frac{-4\pi E_o}{kcZ_o\Omega} \left\{ \cos[k(y-\ell_2)] \sum_{m=1}^{6} \hat{\psi}_{2,m}(k)F_m(k,\theta) \right\}$$

$$\tau_3 = \frac{-4\pi E_o}{kcZ_o\Omega} \left\{ \frac{j \cot \theta \ e^{jkx \cos \theta} D(k)}{\hat{D}(k)} + \cos[k(x-\ell_3)] \sum_{m=1}^{6} \hat{\psi}_{3,m}(k)F_m(k,\theta) \right.$$

$$\left. - \sin[k(x-\ell_3)] \sum_{m=1}^{6} \hat{\psi}_{4,m}(k)F_m(k,\theta) \right\}$$

12

SECTION V
CIRCUMFERENTIAL DISTRIBUTION

The problem of calculating the distribution of current or charge on the surface of an aircraft can be divided conceptually into two parts. The first problem, finding the total axial current and total linear charge density, has been addressed in the previous sections of this report. Once the total current and charge have been found, the problem of finding the detailed circumferential distribution remains. This section presents a simplistic method for solving this problem which is valid in the low-frequency limit and away from junctions and ends, assuming the aircraft is composed of circular cylinders.

Following the method of Smythe [ref. 4], suppose that the currents in an infinite cylindrical shell of radius a are everywhere parallel to the axis and can be written in the harmonic series

$$i_z(\phi) = i_o + \sum_{n=1}^{\infty} (C_n \cos n\phi + D_n \sin n\phi)$$

where $\phi = 0$ is the direction of the external $\underline{H}$-field. Then the vector potential inside the cylinder at (r, ϕ) is

$$A_z = -\mu_o a\, i_o \ln a + \frac{\mu_o a}{2} \sum_{n=1}^{\infty} \frac{1}{n} \left(\frac{r}{a}\right)^n \left(C_n \cos n\phi + D_n \sin n\phi\right)$$

and the $\underline{H}$-field is

$$\underline{H} = \frac{1}{\mu_o} \underline{\nabla} \times \underline{A} = \frac{1}{\mu_o} \left[\left(\frac{1}{r}\frac{\partial}{\partial \phi} A_z\right)\hat{r} - \left(\frac{\partial}{\partial r} A_z\right)\hat{\phi} \right]$$

$$= \frac{1}{2} \sum_{n=1}^{\infty} \left(\frac{r}{a}\right)^{n-1} (-C_n \sin n\phi + D_n \cos n\phi)\hat{r}$$

$$- \frac{1}{2} \sum_{n=1}^{\infty} \left(\frac{r}{a}\right)^{n-1} (C_n \cos n\phi + D_n \sin n\phi)\hat{\phi}$$

13

If an incident $\underline{H}$-field of the form $\underline{H}^{inc} = H_o \hat{x}$ is imposed, the internal total $\underline{H}$-field is

$$\underline{H}_T = \left[H_o \cos \phi + \frac{1}{2} \sum_{n=1}^{\infty} \left(\frac{r}{a} \right)^{n-1} (-C_n \sin n \phi + D_n \cos n \phi) \right] \hat{r}$$

$$+ \left[-H_o \sin \phi - \frac{1}{2} \sum_{n=1}^{\infty} \left(\frac{r}{a} \right)^{n-1} (C_n \cos n \phi + D_n \sin n \phi) \right] \hat{\phi}$$

Since $\underline{H}^{inc}$ is actually a slowly-varying field, eddy currents will tend to cancel $\underline{H}^{inc}$ in the interior of the cylinder. Consequently,

$$C_n = 0 \qquad n = 1, \infty$$

$$D_1 = -2H_o$$

$$D_n = 0 \qquad n = 2, \infty \quad .$$

The current density at any point is

$$i_z(\phi) = i_o - 2H_o \sin \phi \quad .$$

A quasi-electrostatic problem gives the surface charge density at any given point as

$$\sigma(\phi) = \sigma_o + \sum_{n=1}^{\infty} (C_n' \cos n \phi + D_n' \sin n \phi)$$

where the derivation is similar to that for the current density. The ϕ-independent terms can be calculated from the total current and linear charge density:

$$a \int_0^{2\pi} i_z(\phi) d\phi = I_{TOTAL} = 2\pi a i_o$$

$$a \int_0^{2\pi} \sigma(\phi) d\phi = \tau_{TOTAL} = 2\pi a \sigma_o$$

14

The axial current distribution and surface charge distribution can thus be written as the sum of the solution of an appropriate local quasi-static boundary-value problem, and the solution of the global problem of matching total axial currents and quasi-static potentials at junctions. For low frequencies, that is to say, frequencies well below the first aircraft resonance, the local term will be important. This is especially true for the current density, since the global contribution is $O(k)$ while the local contribution is $O(1)$. Around the first several aircraft resonances, the global term will dominate the local term. Beyond the first several aircraft resonances, both the simple quasi-static local solution and the stick model global solution break down as the radii of the sticks become comparable to the wavelength of the incident field.

This section is intended primarily as an example of how the circumferential distributions of current and charge can be found from the solution of a local problem once the total axial current and total linear charge density are known. The modeling of aircraft surfaces by circular cylinders introduces only a small error in the global problem, but it greatly influences the local problem. To solve the more general case of a specific cross-sectional shape, one must solve two two-dimensional quasi-magnetostatic problems. The solution of the first problem will give the distribution of the net total charge (or total current; they are the same by Thomson's Theorem) around the circumference of the air-craft section of interest. In the case of the circular cylinder previously mentioned, the distribution is uniform. The second problem is a magnetostatic integral equation for the current density which is solved using the incident magnetic field as the driving term. The solutions of these two local problems will depend strongly on the local geometry. Therefore, it is not intended that the specific results of this section should be used for any actual case, except perhaps as the first step in a more rigorous calculation or as a check of the final results.

15

SECTION VI

NUMERICAL RESULTS AND CONCLUSIONS

Figures 2 - 19 are plots of the magnitude of the total axial current and total linear charge density for several points of interest on the B-1, E-4, and EC-135 aircraft, for topside incidence ($\theta = 90°$) . Figure 20 is a superposition of the current plots in figures 2 and 4 so that a direct comparison can be more easily made between the current on the forward section of the B-1 fuselage and the current on the aft section of the fuselage. As discussed in reference 1, the fundamental resonance of the aircraft dominates the behavior of the current and charge on the aft section of the fuselage. The second resonance, which involves primarily the forward section of the fuselage and the wings, is very important on the forward section of the fuselage but is virtually unseen on the aft section. These features are shown clearly in figure 20 for the B-1 aircraft. Figures 8, 10, 14, and 16 show the same phenomenon for the E-4 and EC-135 aircraft.

Figure 21 is a comparison of the magnitude of the average current density ($J = H = I/2\pi a$; $a = .5$ meters) at the mid point of the forward fuselage of the B-1 as calculated using the computer code in appendix B and using the thin-wire computer code described in reference 5. The agreement is good; in fact, for all features of the two curves except the first resonance, the agreement is remarkably good. The thin-wire computer code gives a higher peak at the first resonance than would be expected using the arguments of the previous paragraph.

The current and charge transfer functions as presented in this report offer significant advantages over those previously available. Because they are essentially closed-form results, they offer the computational advantages of speed and minimal memory requirements (no matrices to invert, for instance), as well as the possibility of straightforward analytic inversion into the time domain. In addition, the availability of reasonably simple analytic expressions for the current and charge transfer functions greatly simplifies the problem of synthesis by equivalent networks. Inversion into the time domain and network synthesis are appropriate subjects for future study.

The weakness of this method of calculating the current and charge transfer functions is that it ignores the problem of local geometry. The circumferential distributions of the current and charge densities must be found by solving a local boundary-value problem specific to the exact location on the particular aircraft under study. That task is beyond the scope of this report. However, knowledge of the total current and total linear charge density is a necessary first step in the determination of the circumferential distributions of the current and charge densities.
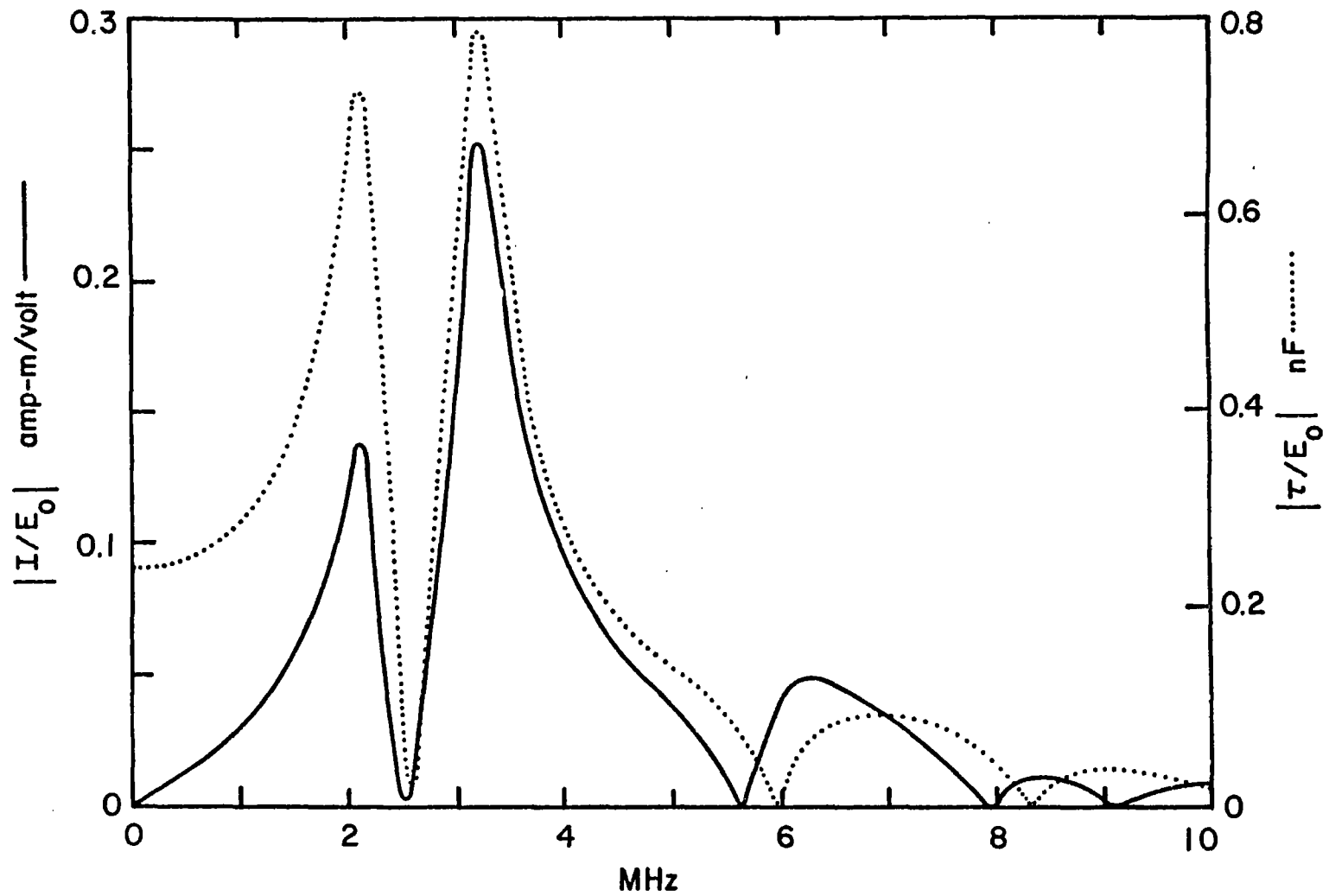
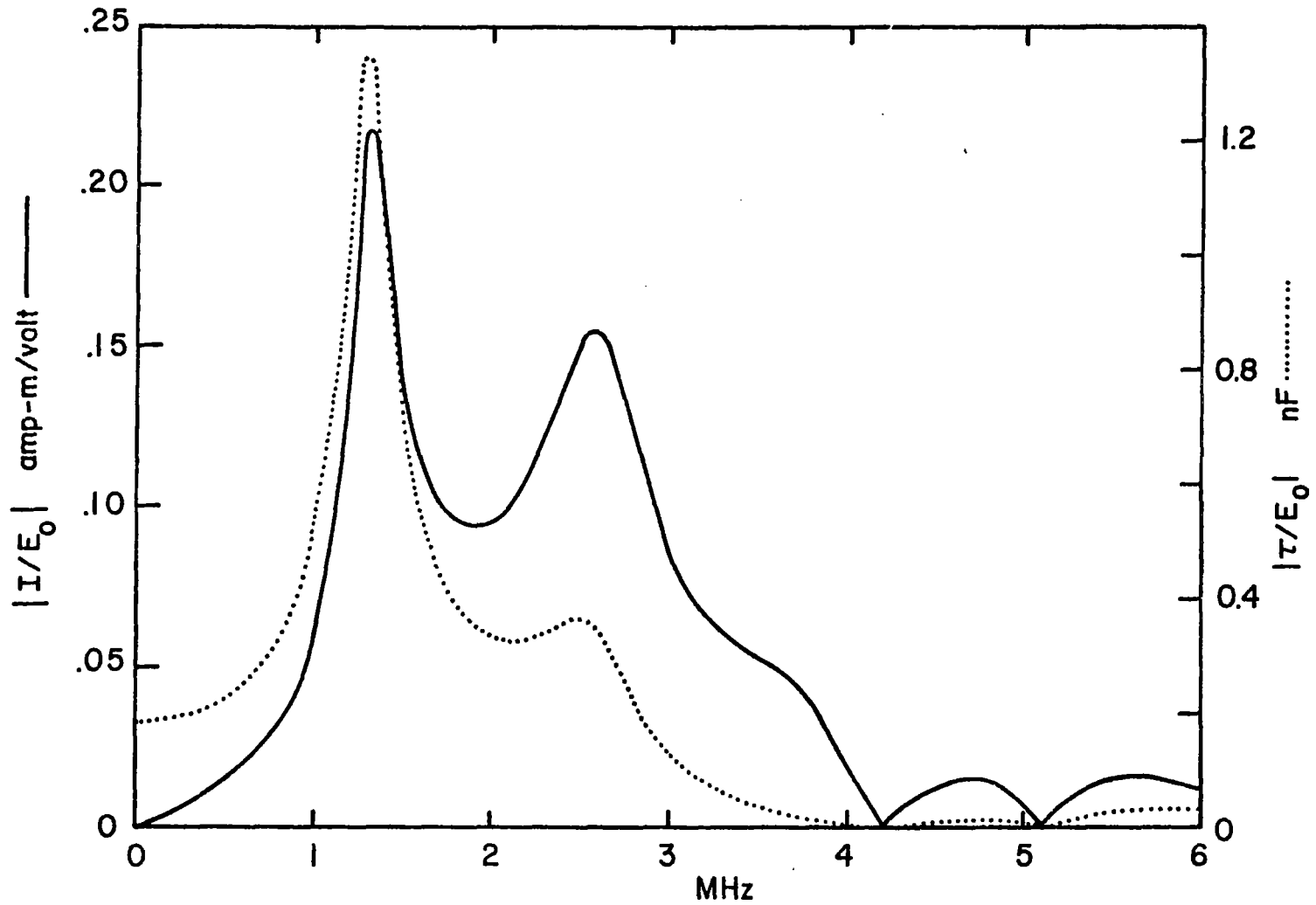Figure 2. Total current and charge density on the mid forward fuselage of the B-1 for topside incidence.
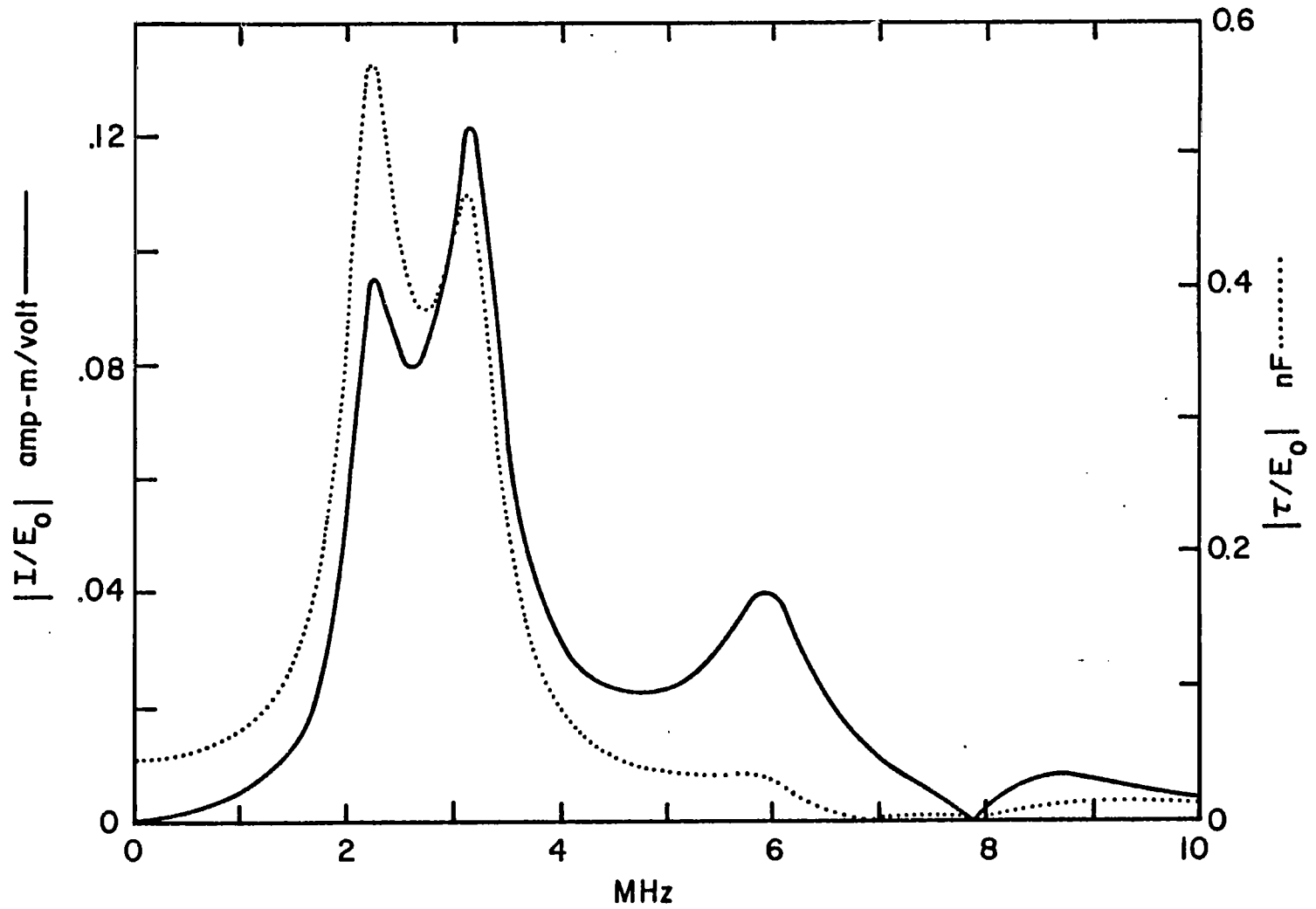
Figure 3. Total current and charge density on the mid wing of the B-1 for topside incidence.
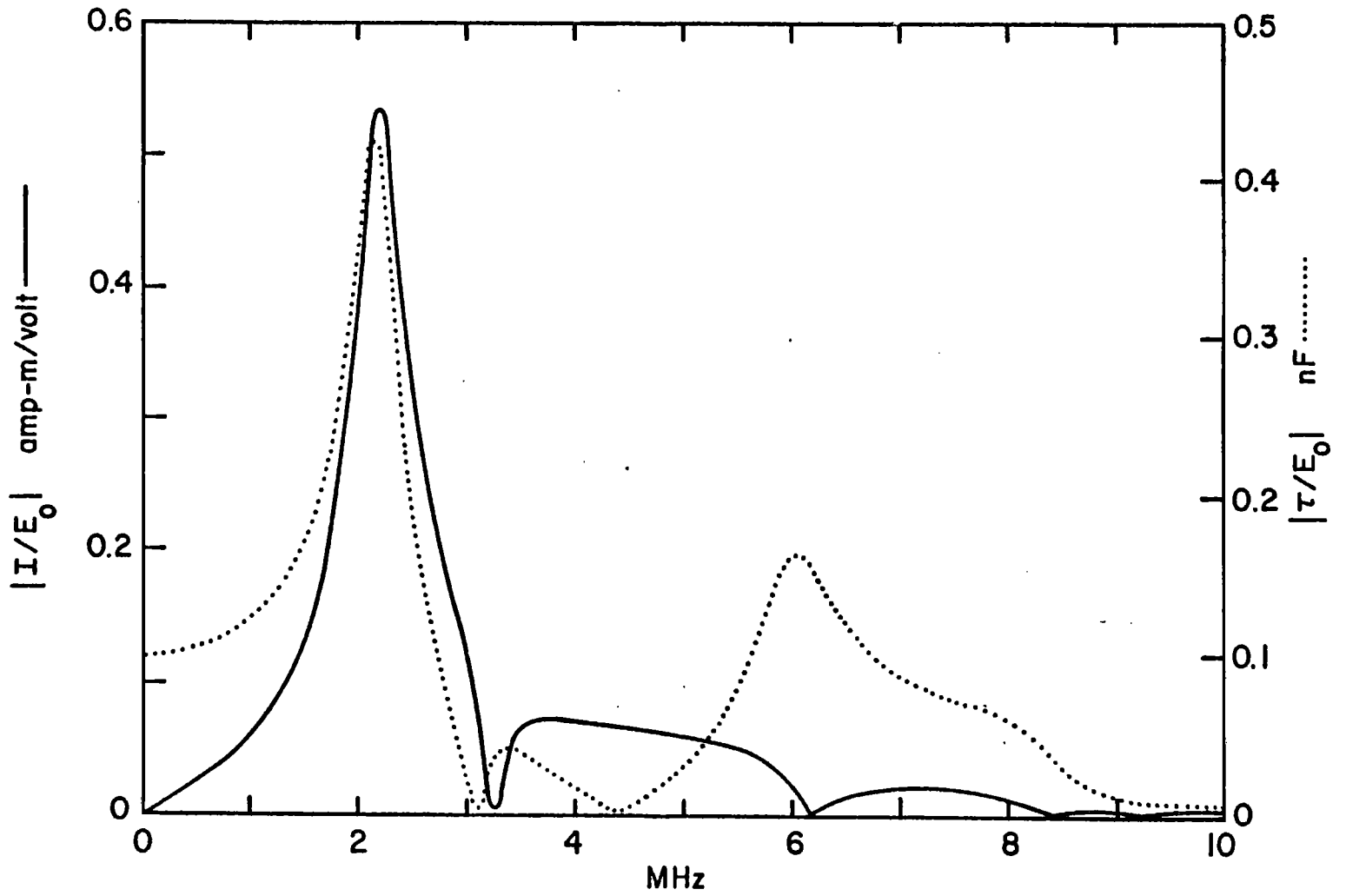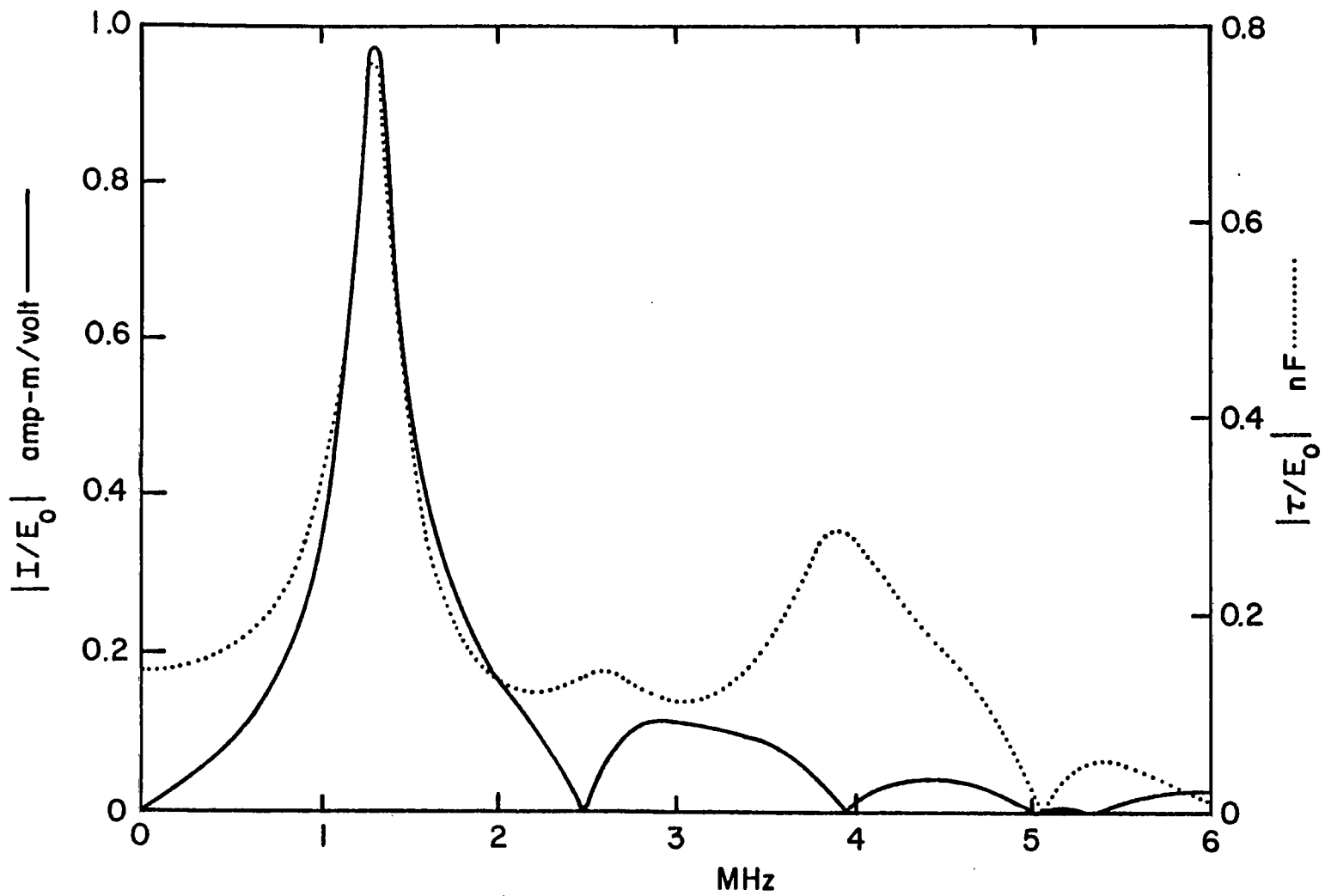
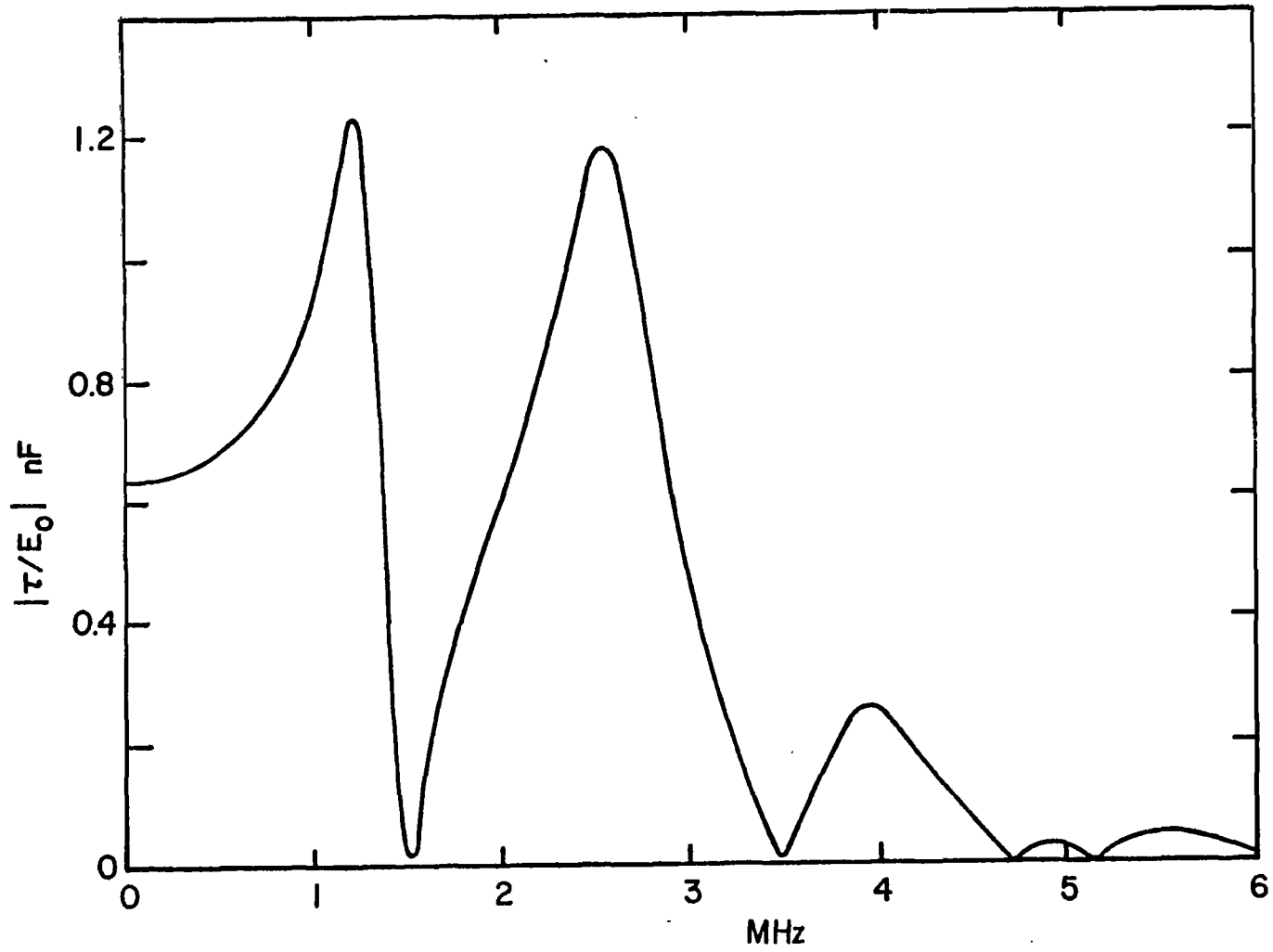Figure 4. Total current and charge density on the mid aft fuselage of the B-1 for topside incidence.
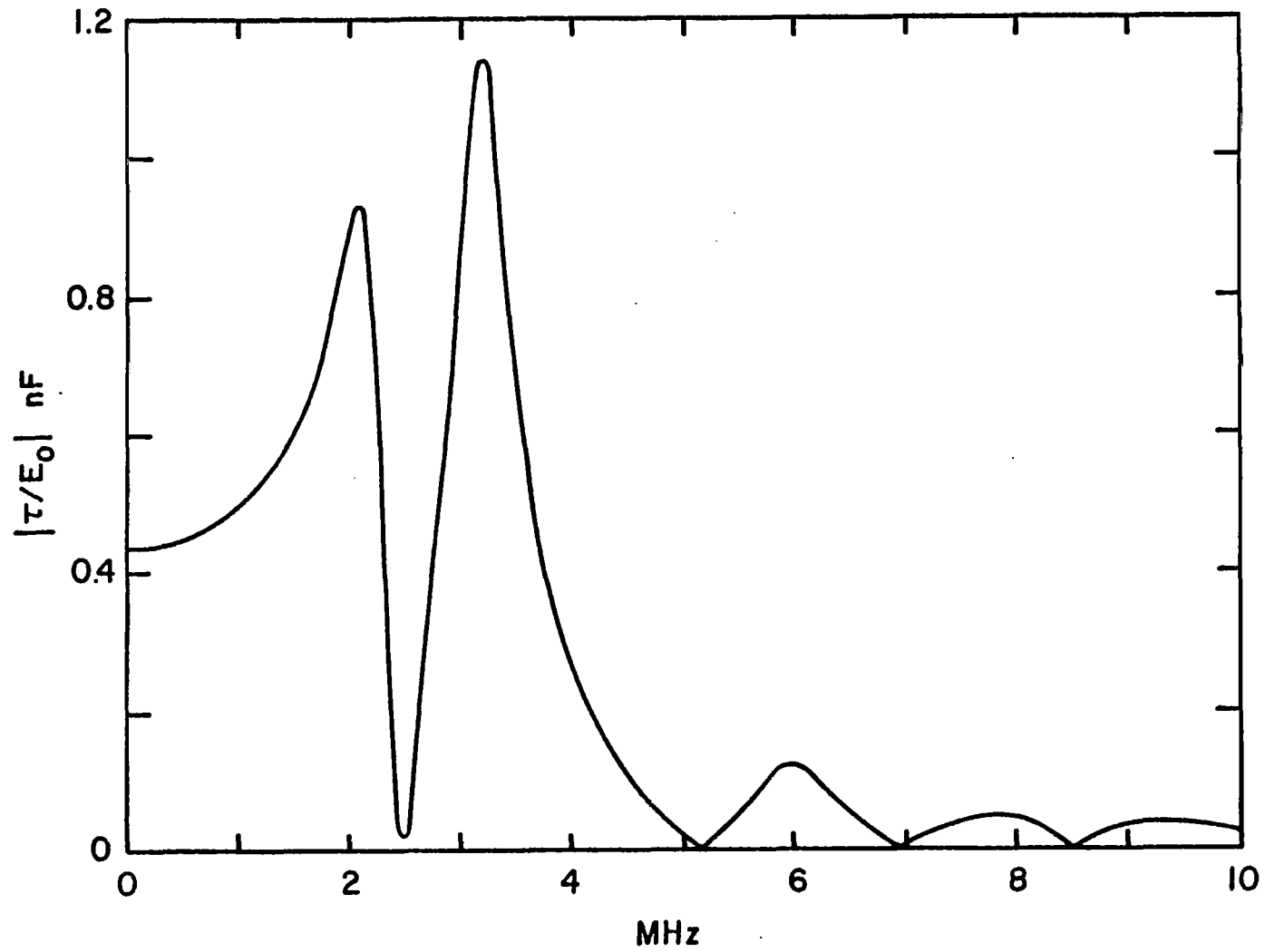
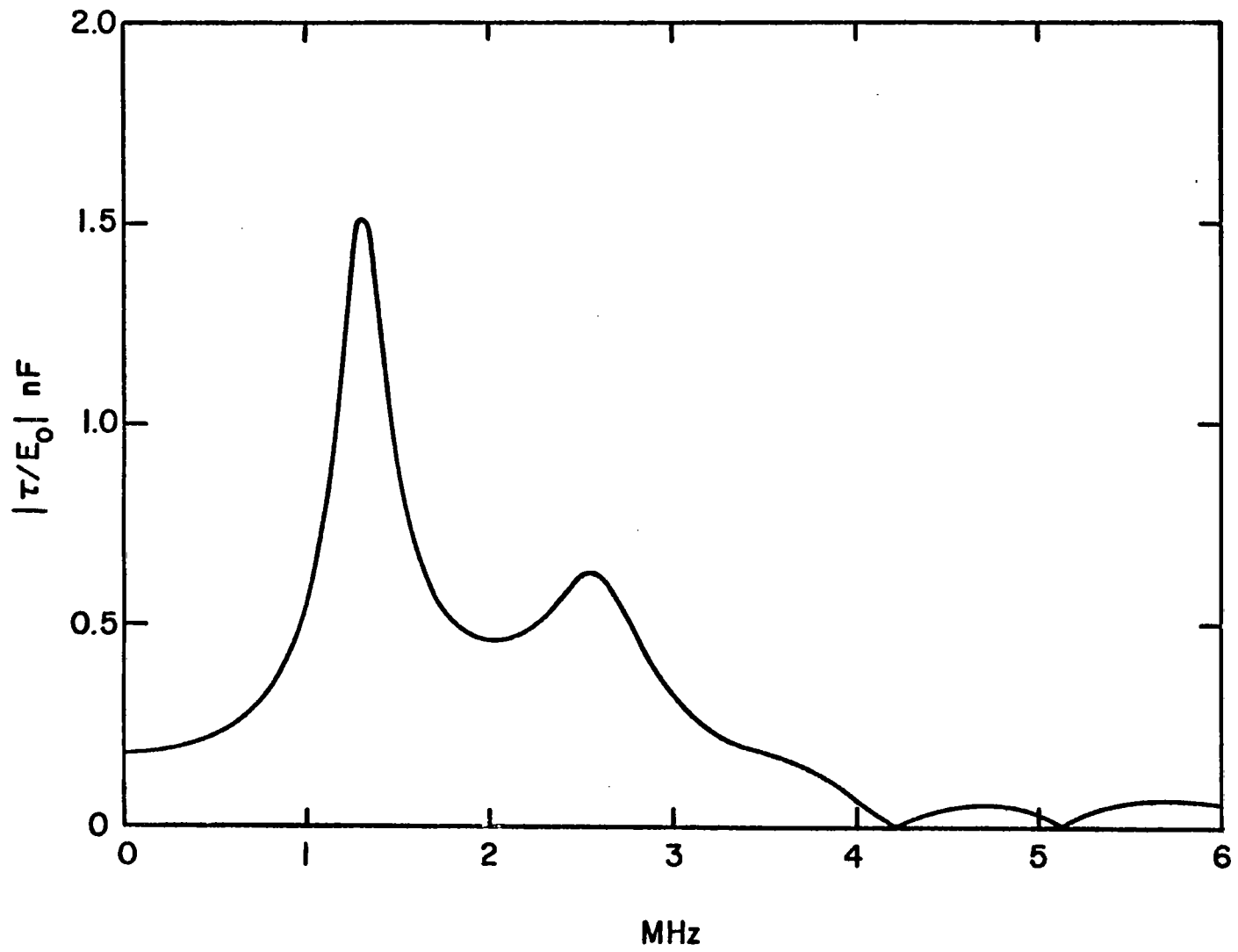Figure 5.   Linear charge density on the B-1 at the nose for topside incidence.
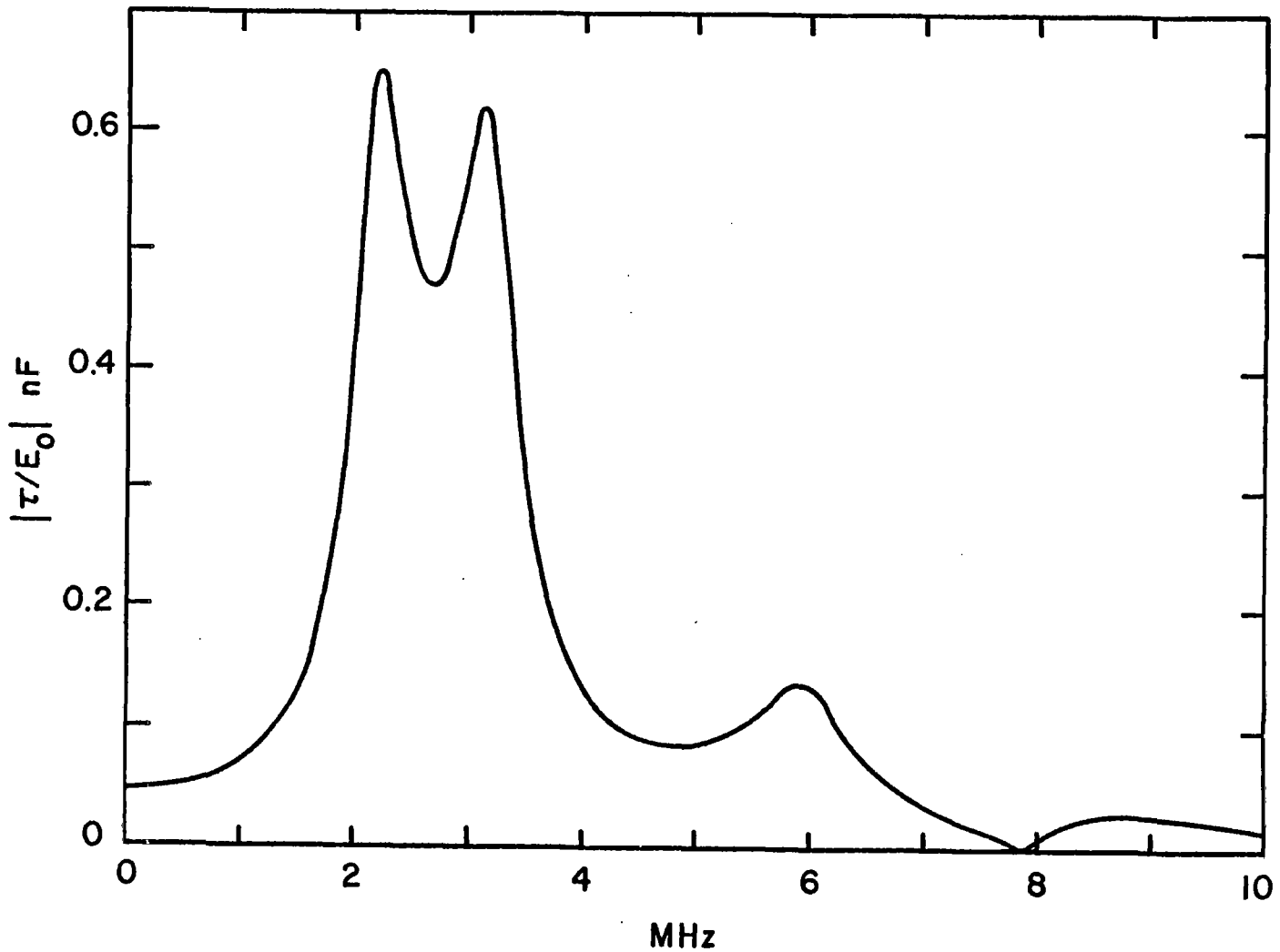
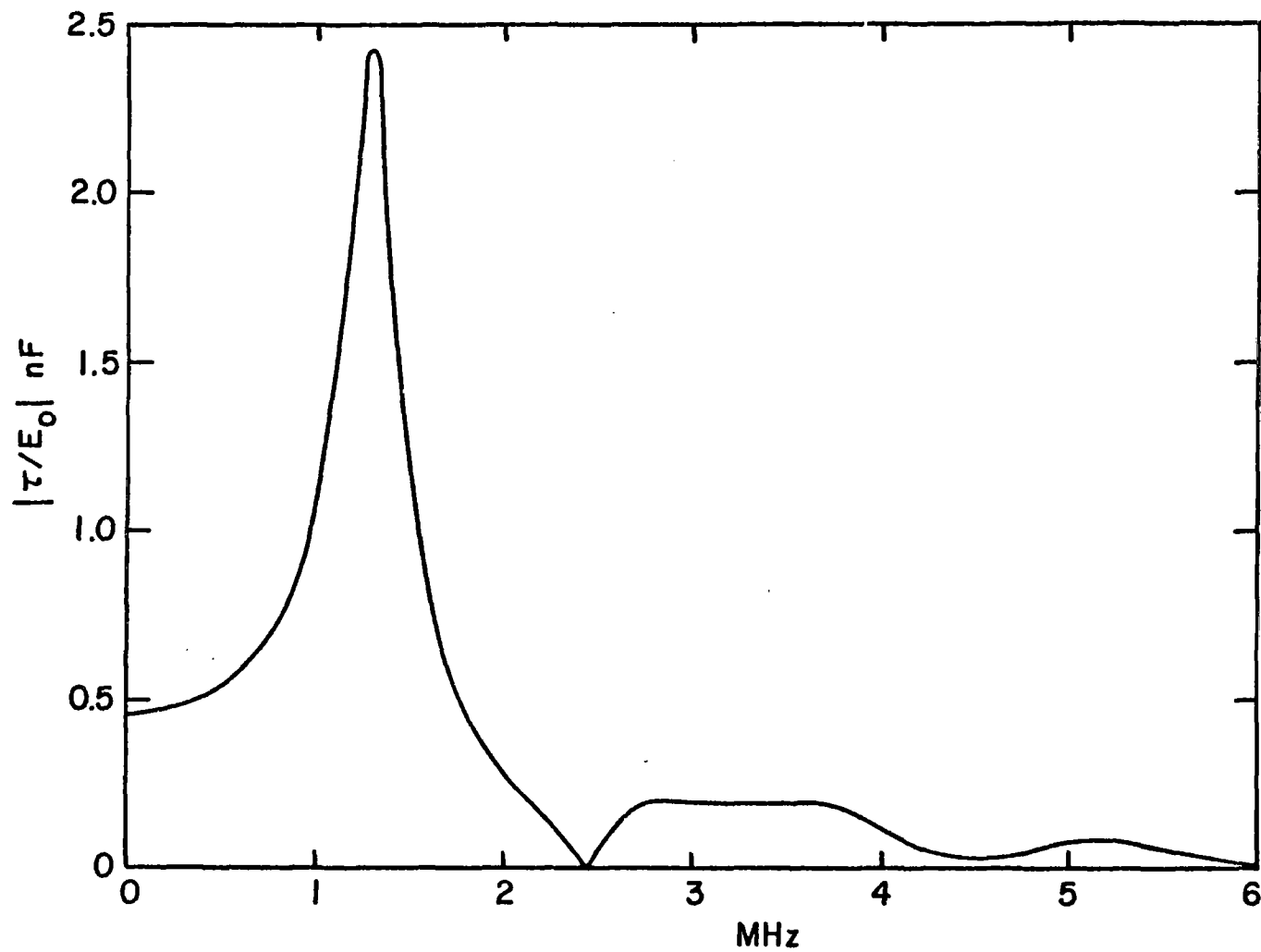Figure 6.   Linear charge density on the B-1 at the wing tip for topside incidence.
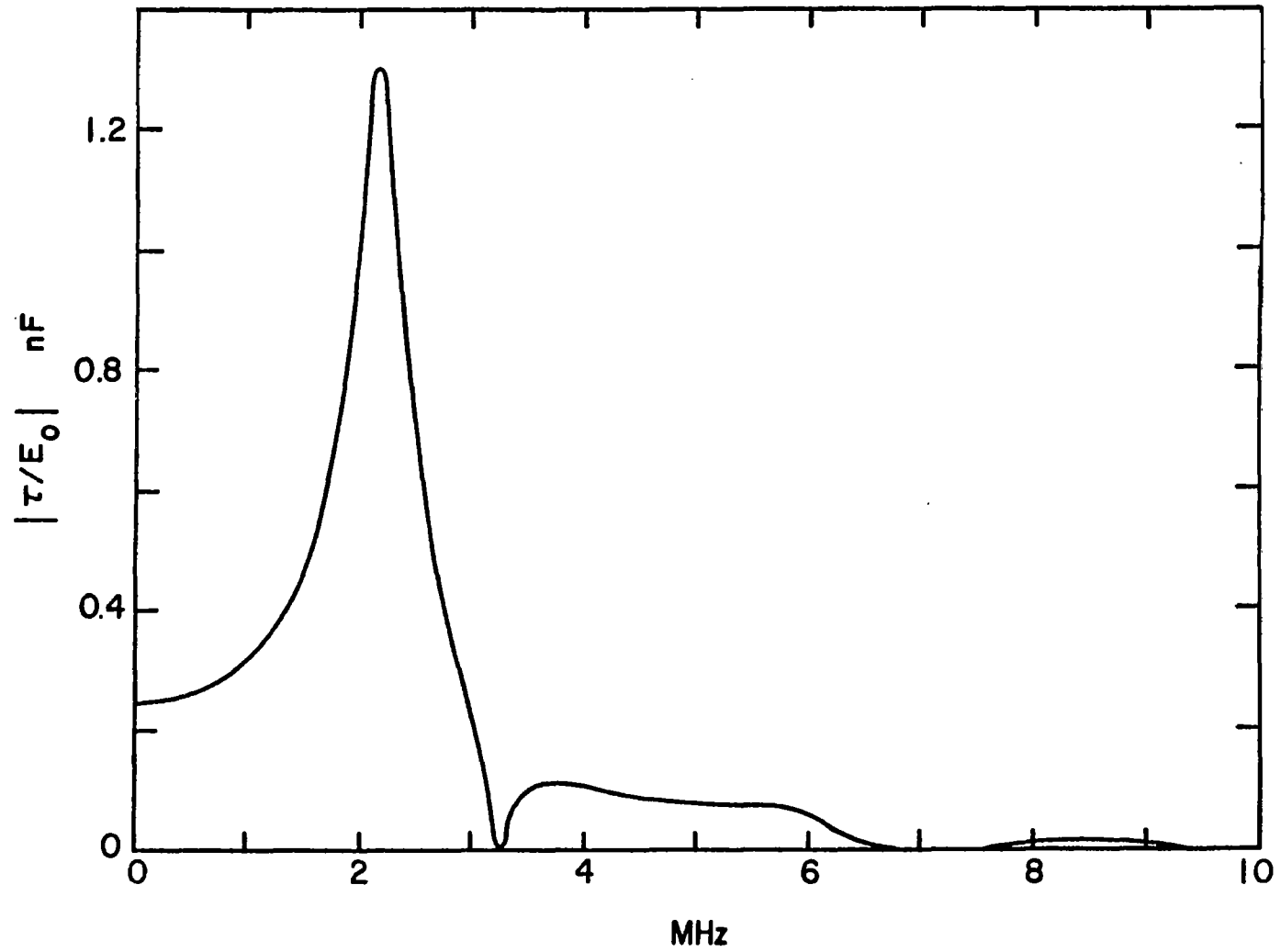
Figure 7. Linear charge density on the B-1 at the top of the vertical stabilizer for topside incidence.

23
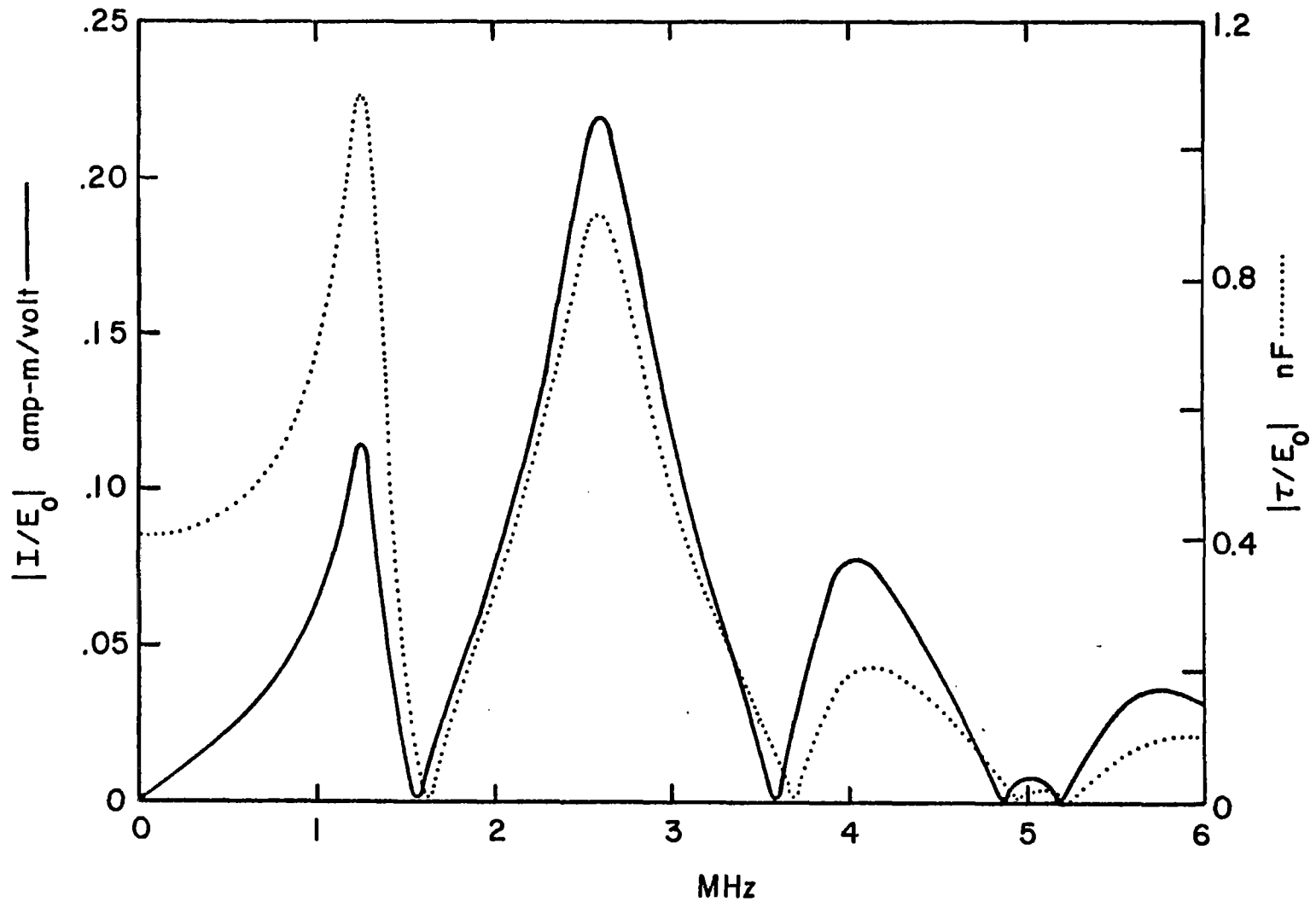
Figure 8.   Total current and charge density on the mid forward fuselage of the E-4 for topside incidence.

Figure 9. Total current and charge density on the mid wing of the E-4 for topside incidence.

Figure 10. Total current and charge density on the mid aft fuselage of the E-4 for topside incidence.

Figure 11. Linear charge density on the E-4 at the nose for topside incidence.

Figure 12.   Linear charge density on the E-4 at the wing tip for topside incidence.

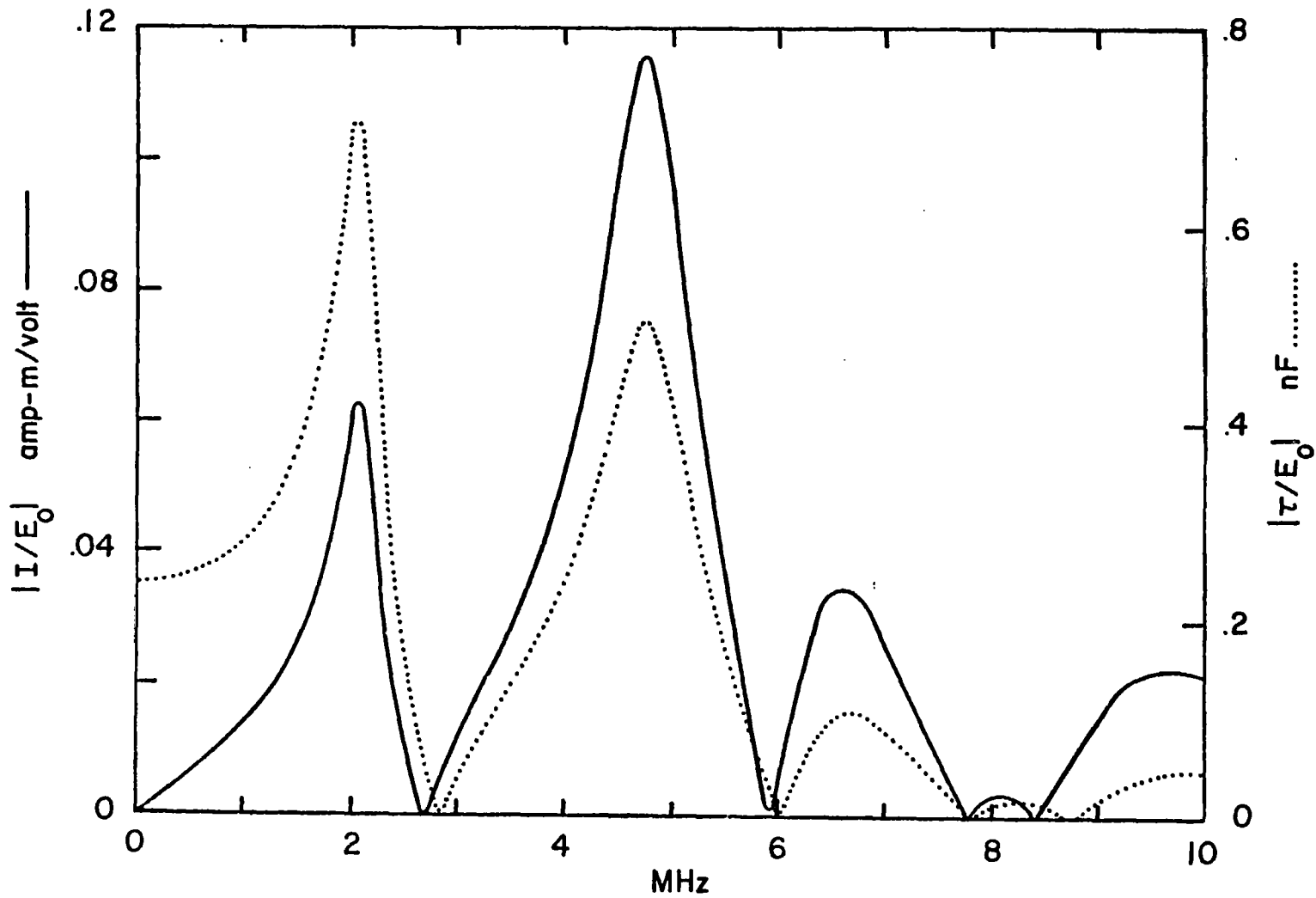Figure 13. Linear charge density on the E-4 at the top of the vertical stabilizer for topside incidence.

Figure 14. Total current and charge density on the mid forward fuselage of the EC-135 for topside incidence.
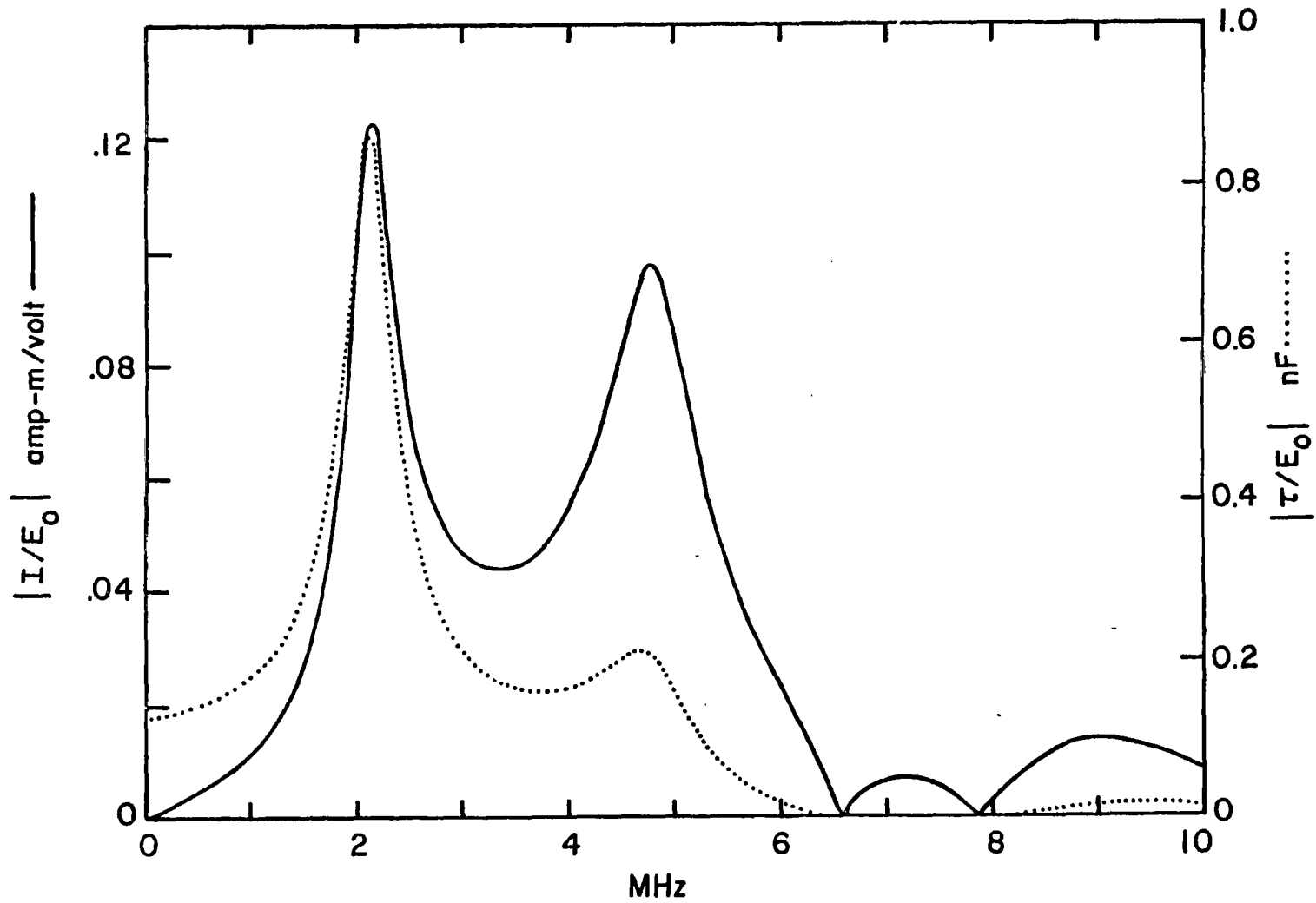
Figure 15. Total current and charge density on the mid wing of the EC-135 for topside incidence.
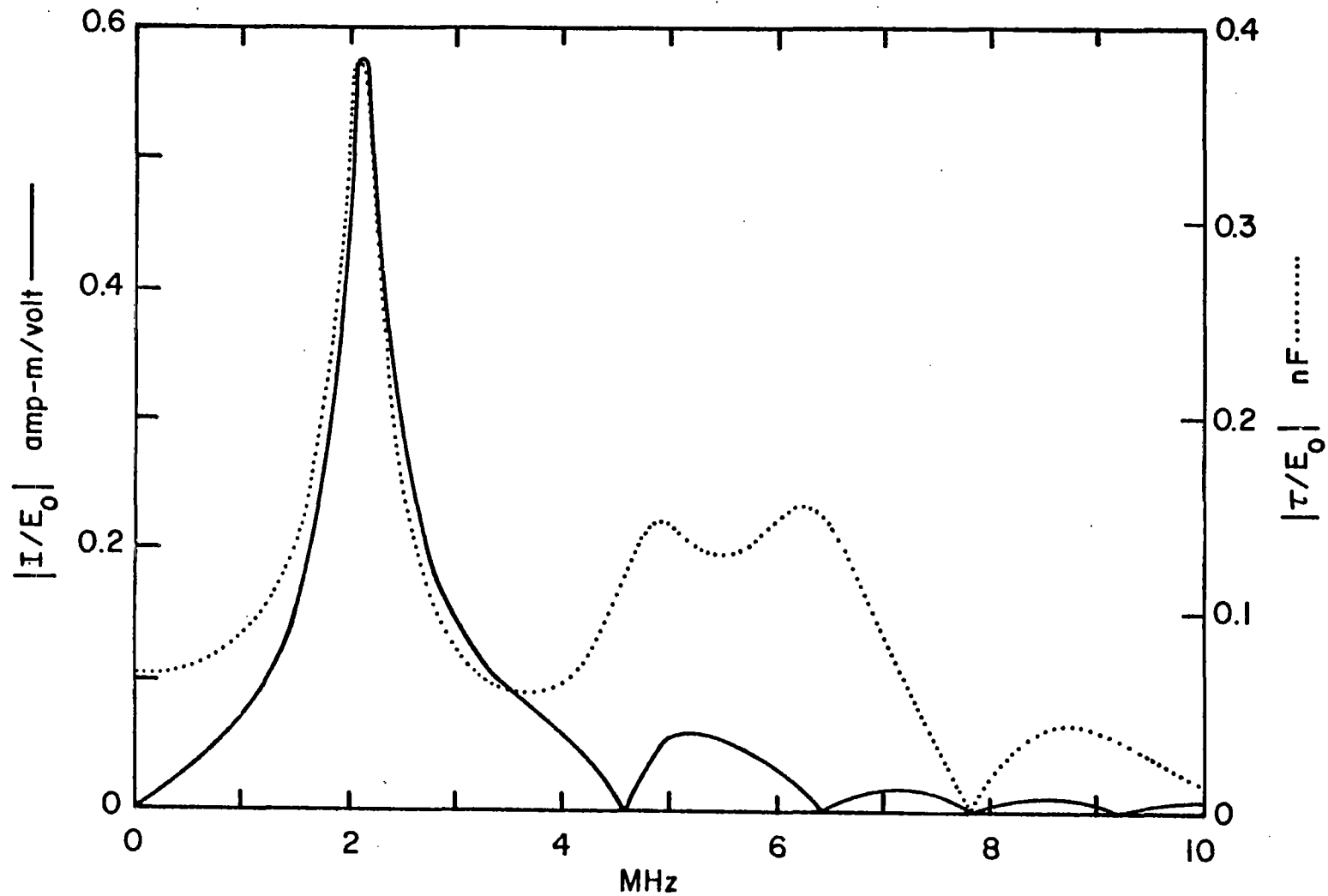
Figure 16. Total current and charge density on the mid aft fuselage of the EC-135 for topside incidence.
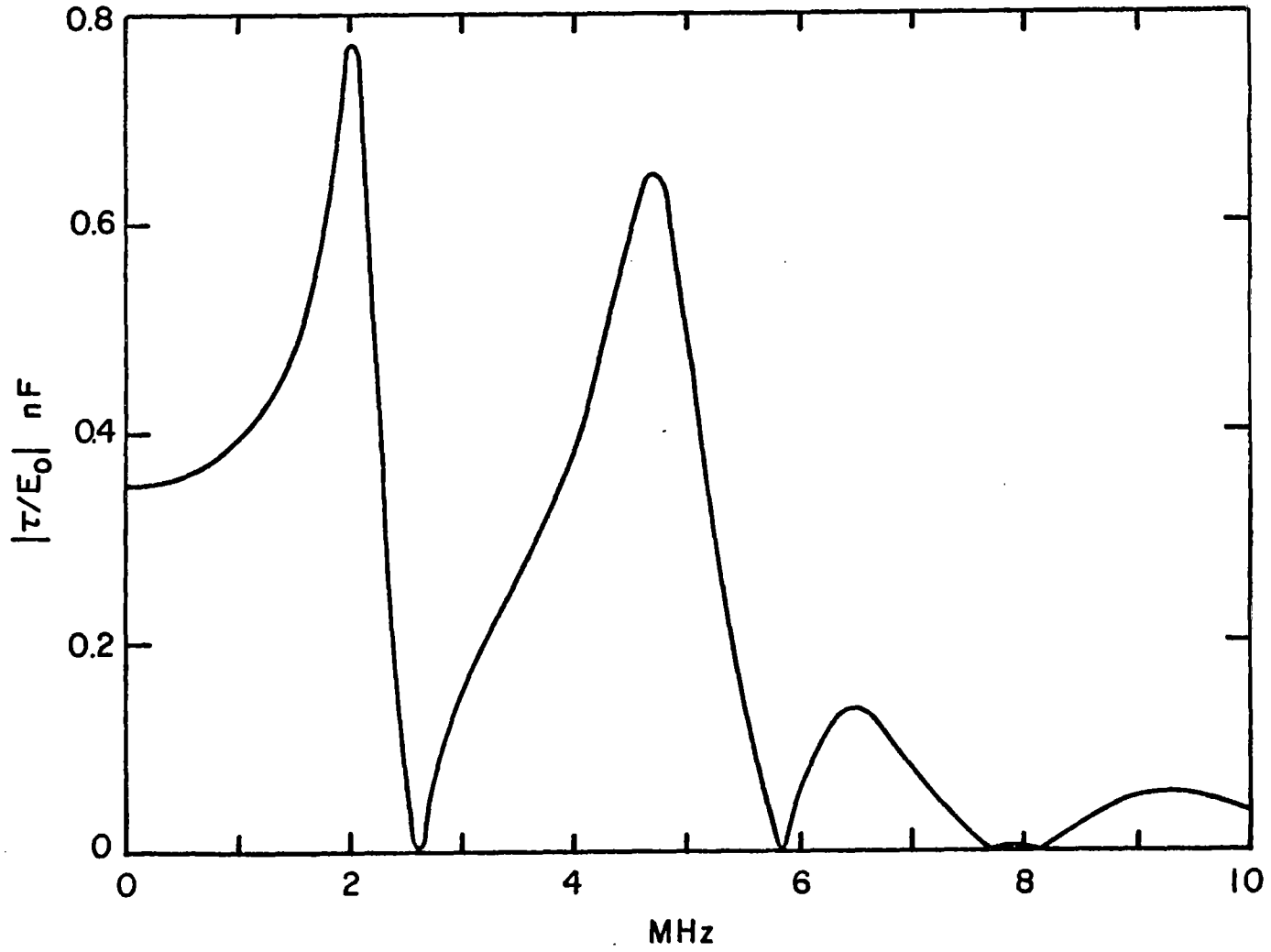
32

Figure 17. Linear charge density on the EC-135 at the nose for topside incidence.
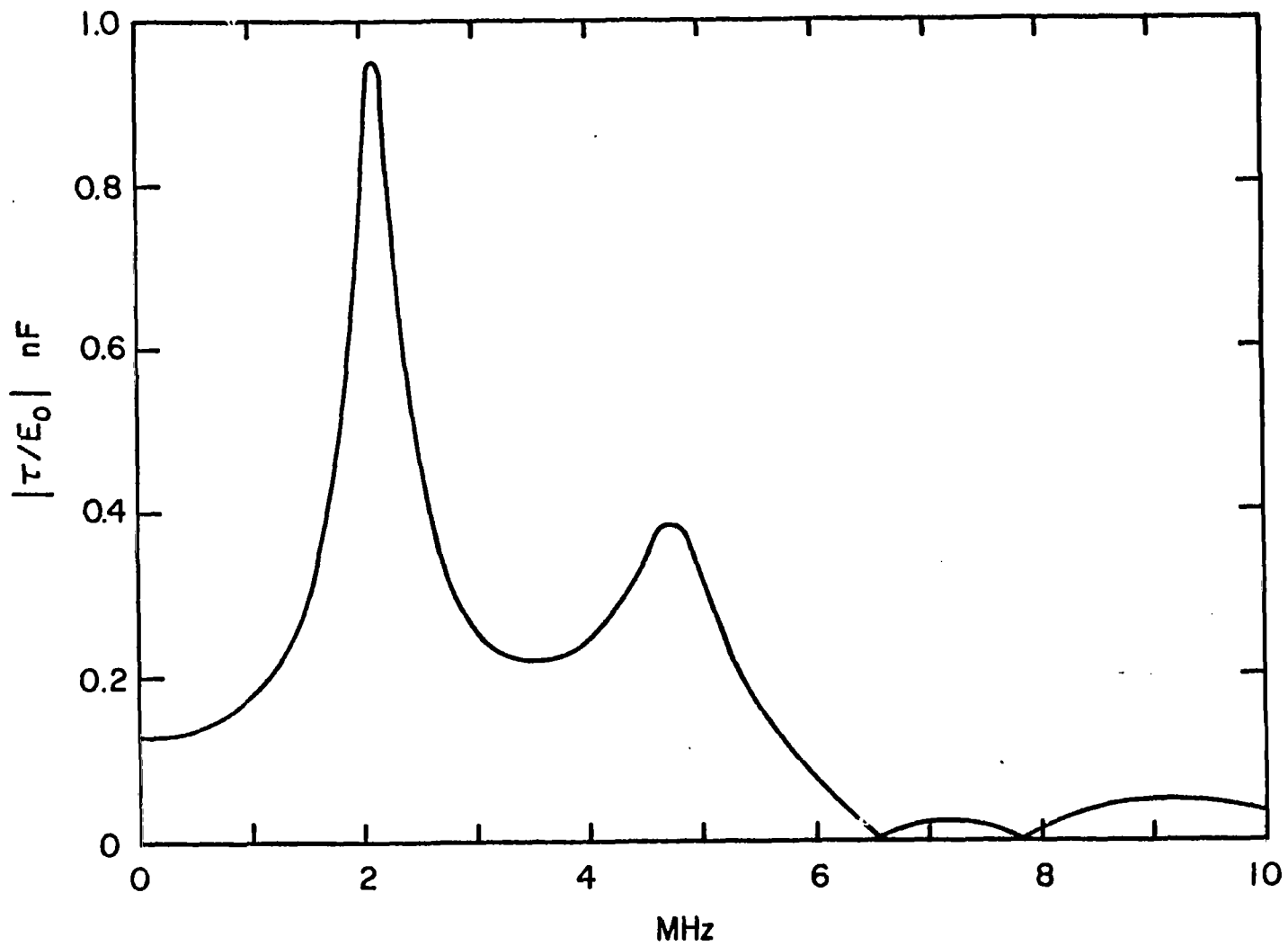
33

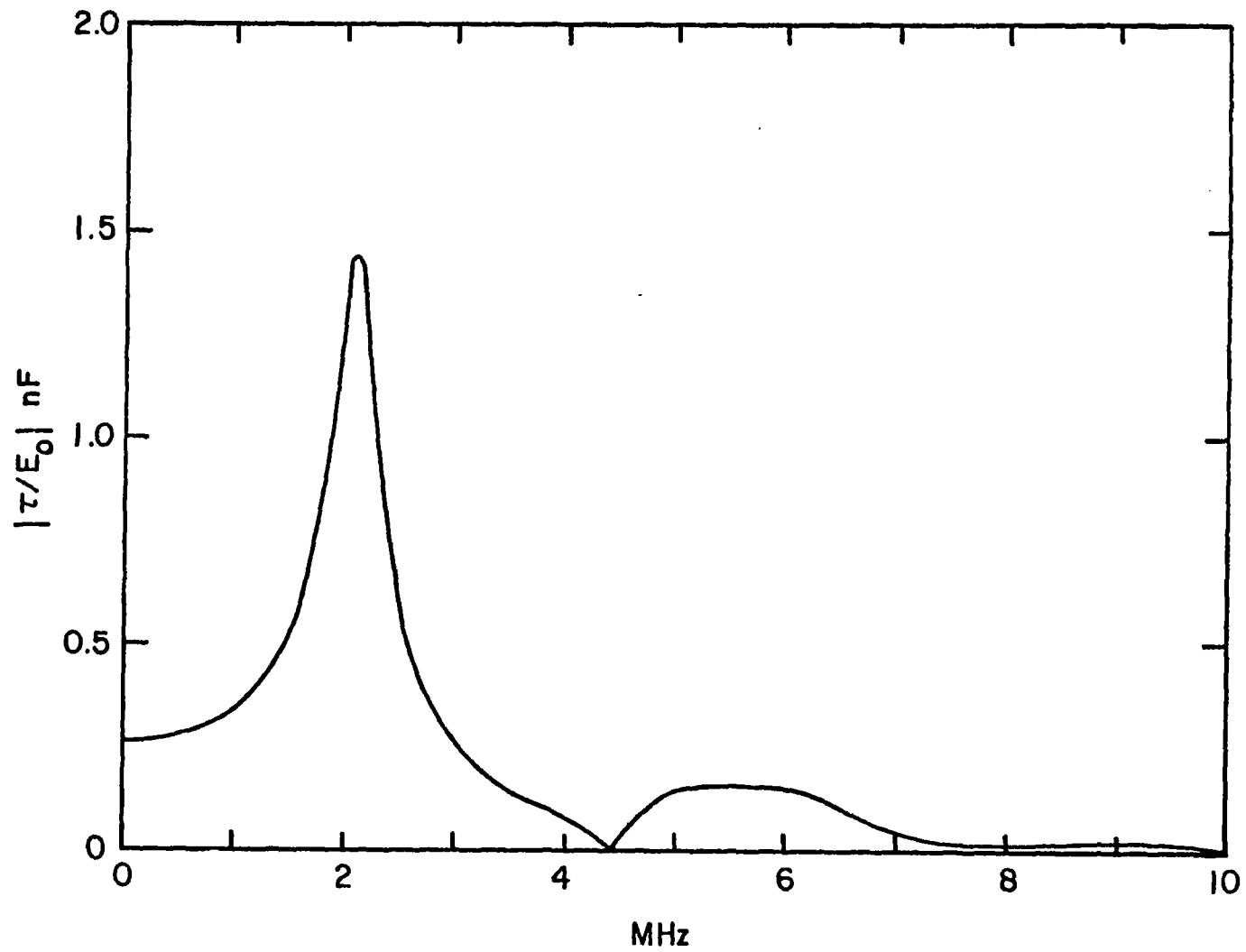Figure 18. Linear charge density on the EC-135 at the wing tip for topside incidence.

Figure 19. Linear charge density on the EC-135 at the top of the vertical stabilizer for topside incidence.
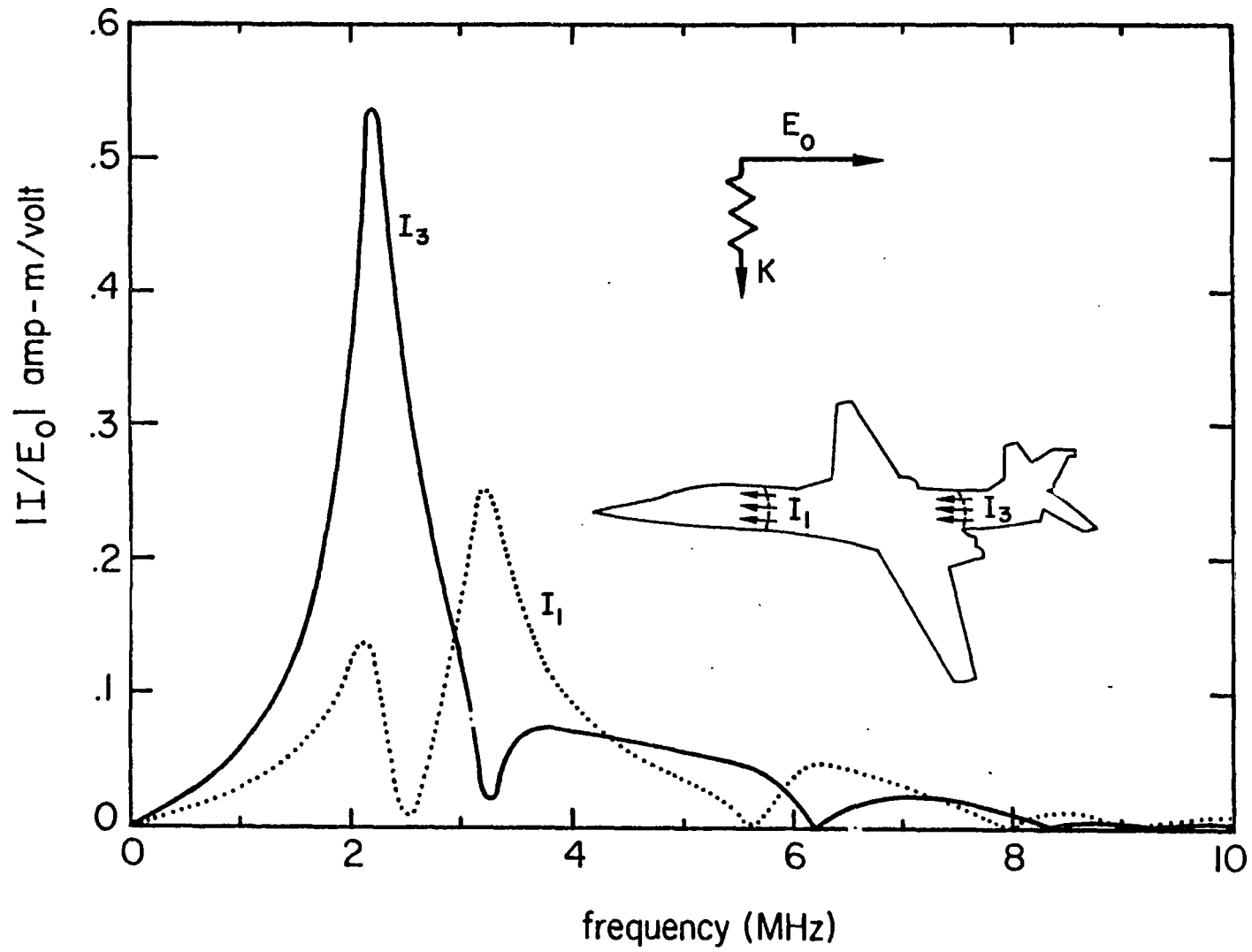
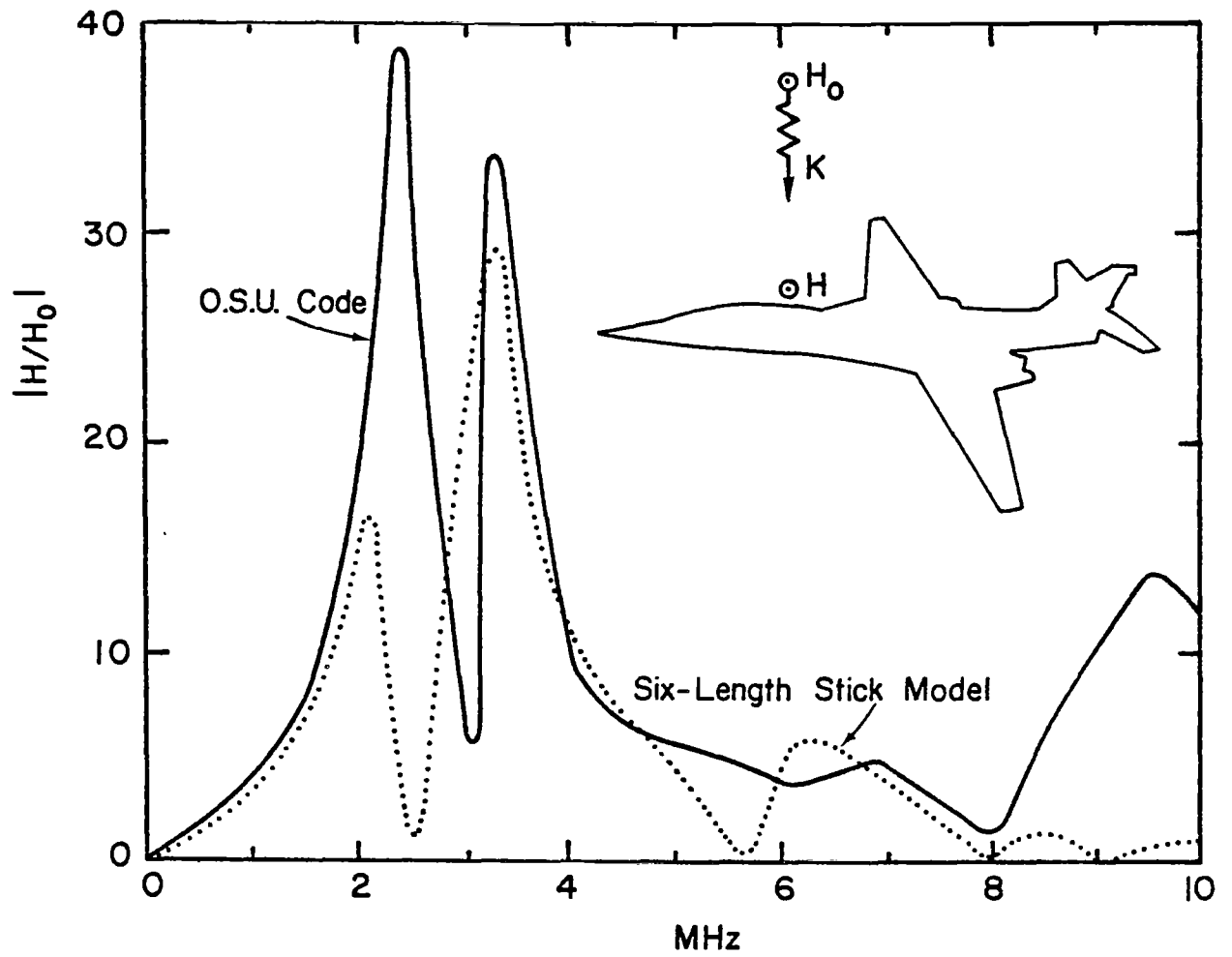Figure 20. Comparison of total current on the mid forward and mid aft fuselage of the B-1.

Figure 21. Comparison of O.S.U. thin-wire computer code with six-length stick model for B-1 forward fuselage, topside incidence.

37

APPENDIX A

The following are the explicit expressions for the ψ-functions of equations (3) in section II. Let

$$D(k) = \cos k\ell_1 \cos k\ell_2 \cos k(\ell_3+\ell_4) \cos k\ell_5 \cos k\ell_6$$

$$\times [\tan k\ell_1 + 2 \tan k\ell_2 + \tan k(\ell_3+\ell_4) + 2 \tan k\ell_5 + \tan k\ell_6$$

$$- (\tan k\ell_1 + 2 \tan k\ell_2) \tan k(\ell_3+\ell_4)(2 \tan k\ell_5 + \tan k\ell_6)]$$

Then

$$D(k)\psi_{1,1} = \cos k\ell_1 \cos k\ell_2 \cos k(\ell_3+\ell_4) \cos k\ell_5 \cos k\ell_6$$

$$\times \{-1 + \tan k(\ell_3+\ell_4)(2 \tan k\ell_5 + \tan k\ell_6)$$

$$+ \tan k\ell_1 [2 \tan k\ell_2 + \tan k(\ell_3+\ell_4) + 2 \tan k\ell_5 + \tan k\ell_6$$

$$- 2 \tan k\ell_2 \tan k(\ell_3+\ell_4)(2 \tan k\ell_5 + \tan k\ell_6)]\}$$

$$D(k)\psi_{1,2} = \cos k\ell_2 \cos k(\ell_3+\ell_4) \cos k\ell_5 \cos k\ell_6$$

$$\times \{\tan k\ell_2 [\tan k(\ell_3+\ell_4)(2 \tan k\ell_5 + \tan k\ell_6) - 1]\}$$

$$D(k)\psi_{1,3} = \cos k\ell_2 \cos k\ell_5 \cos k\ell_6$$

$$\times \{\sin k\ell_4 (2 \tan k\ell_5 + \tan k\ell_6) - \cos k\ell_4\}$$

$$D(k)\psi_{1,4} = \cos k\ell_2 \cos k\ell_5 \cos k\ell_6$$

$$\times \{\cos k\ell_4 (2 \tan k\ell_5 + \tan k\ell_6) + \sin k\ell_4\}$$

$$D(k)\psi_{1,5} = \cos k\ell_2 \sin k\ell_5 \cos k\ell_6$$

38

$$D(k)\psi_{1,6} = \cos k\ell_2 \cos k\ell_5$$

$$D(k)\psi_{2,1} = \cos k(\ell_3+\ell_4)\cos k\ell_5 \cos k\ell_6$$

$$\times \{\tan k(\ell_3+\ell_4)(2\tan k\ell_5 + \tan k\ell_6) - 1\}$$

$$D(k)\psi_{2,2} = \tfrac{1}{2}\cos k\ell_1 \cos k(\ell_3+\ell_4)\cos k\ell_5 \cos k\ell_6$$

$$\times \{\tan k\ell_1 + \tan k(\ell_3+\ell_4) + 2\tan k\ell_5 + \tan k\ell_6$$

$$- \tan k\ell_1 \tan k(\ell_3+\ell_4)(2\tan k\ell_5 + \tan k\ell_6)\}$$

$$\psi_{2,m} = \frac{\cos k\ell_1 \psi_{1,m}}{\cos k\ell_2} \qquad m = 3,6$$

$$\psi_{3,1} = \cos k\ell_2 \psi_{2,1}$$

$$\psi_{3,m} = \cos k\ell_1 \psi_{1,m} \qquad m = 2,6$$

$$D(k)\psi_{4,1} = - \cos k\ell_2 \cos k(\ell_3+\ell_4)\cos k\ell_5 \cos k\ell_6$$

$$\times \{\tan k(\ell_3+\ell_4) + 2\tan k\ell_5 + \tan k\ell_6\}$$

$$D(k)\psi_{4,2} = - \sin k\ell_2 \cos k(\ell_3+\ell_4)\cos k\ell_5 \cos k\ell_6$$

$$\times \{\tan k(\ell_3+\ell_4) + 2\tan k\ell_5 + \tan k\ell_6\} \times \cos k\ell_1$$

$$\psi_{4,m} = - (\tan k\ell_1 + 2\tan k\ell_2)\cos k\ell_1 \psi_{1,m} \qquad m = 3,6$$

REFERENCES

[1] G. Bedrosian, "Stick-Model Characterization of the Natural Frequencies and Natural Modes of Aircraft," Interaction Note 326, Air Force Weapons Laboratory, Kirtland AFB, New Mexico, 14 September 1977.

[2] L. Marin, "Currents Induced on the VLF/LF Antenna Wires on the E-4 in the Resonance Region of the Aircraft," DAA Memo 31, Air Force Weapons Laboratory, Kirtland AFB, New Mexico, December 1976.

[3] E.T. Whittaker and G.N. Watson, A Course of Modern Analysis, Cambridge University Press, New York (1965).

[4] W.R. Smythe, Static and Dynamic Electricity, McGraw-Hill Book Company, New York (1968).

[5] T.L. Brown, "Application of a Wire Computer Code to the B-1 Aircraft," AFWL-TR-75-226, Air Force Weapons Laboratory, Kirtland AFB, New Mexico, August 1976.

[6] J.P. Castillo, "A Comparison of Aircraft Scale Model Test Results with Predictions," Interaction Application Memo 9, Air Force Weapons Laboratory, Kirtland AFB, New Mexico, September 1975.